JOURNAL OF THE ROYAL SOCIETY Interface

Diamond and biology

Christoph E Nebel, Dongchan Shin, Bohuslav Rezek, Norio Tokuda, Hiroshi Uetsuka and Hideyuki Watanabe

J. R. Soc. Interface 2007 **4**, 439-461
doi: 10.1098/rsif.2006.0196

JOURNAL OF THE ROYAL SOCIETY Interface

J. R. Soc. Interface (2007) **4**, 439–461
doi:10.1098/rsif.2006.0196
Published online 18 January 2007

REVIEW

Diamond and biology

Christoph E. Nebel*, Dongchan Shin, Bohuslav Rezek, Norio Tokuda, Hiroshi Uetsuka and Hideyuki Watanabe

Diamond Research Center, AIST, Central 2, Tsukuba 305-8568, Japan

A summary of photo- and electrochemical surface modifications applied on single-crystalline chemical vapour deposition diamond films is given. The covalently bonded formation of amine and phenyl linker molecular layers is characterized using X-ray photoelectron spectroscopy, atomic force microscopy (AFM), cyclic voltammetry and field-effect transistor characterization experiments. Amine and phenyl layers are very different with respect to formation, growth, thickness and molecular arrangement. We deduce a sub-monolayer of amine linker molecules on diamond with approximately 10% coverage of $1.5\times10^{15}\,\mathrm{cm}^{-2}$ carbon bonds. Amine is bonded only on initially H-terminated surface areas. In the case of electrochemical deposition of phenyl layers, multilayer properties are detected with three-dimensional nitrophenyl growth properties. This leads to the formation of typically 25 Å thick layers. The electrochemical bonding to boron-doped diamond works on H-terminated and oxidized surfaces.

After reacting such films with heterobifunctional cross-linker molecules, thiol-modified ss-DNA markers are bonded to the organic system. Application of fluorescence and AFM on hybridized DNA films shows dense arrangements with densities up to $10^{13}\,\mathrm{cm}^{-2}$. The DNA is tilted by an angle of approximately 35° with respect to the diamond surface. Shortening the bonding time of thiol-modified ss-DNA to 10 min causes a decrease in DNA density to approximately $10^{12}\,\mathrm{cm}^{-2}$. Application of AFM scratching experiments shows threshold removal forces of approximately 75 and 45 nN for the DNA bonded to the phenyl and the amine linker molecules, respectively. First, DNA sensor applications using $\mathrm{Fe(CN_6)}^{3-/4-}$ mediator redox molecules and DNA field-effect transistor devices are introduced and discussed.

Keywords: diamond; biofunctionalization; DNA hybridization detection

1. INTRODUCTION

Genomics research has elucidated many new biomarkers that have the potential to greatly improve disease diagnostics (Sander 2000; Srinivas *et al.* 2001; Etzioni *et al.* 2003). The availability of multiple biomarkers is especially important in the diagnosis of complex diseases like cancer, for which disease heterogeneity makes tests of single markers inadequate (Brawer 2001; Wulfkuhle *et al.* 2003). In addition, the use of markers associated with different stages of disease pathogenesis will facilitate early detection. However, widespread use of markers in healthcare will ultimately depend upon the development of detection techniques that will allow rapid detection of many markers with high selectivity and sensitivity. Therefore, the identification of proper transducer materials, optimization of detection techniques and sensitivities, establishment of biotechnologies for multiarray sensors' realization with dimensions below the micrometre regime and exploration of chemical stability in high-throughput systems attract increasing attention. DNA immobilization techniques have been explored for a variety of substrates like latex beads, polystyrene, carbon electrodes, gold and oxidized silicon or glass (Kremsky *et al.* 1987; Rasmussen *et al.* 1991; Millan *et al.* 1992; Hashimoto *et al.* 1994; Strother *et al.* 2000). These materials do not generally possess all the desired characteristics of an ideal biosurface like flatness, homogeneity, chemical stability, reproducibility and biochemical surface modifications. In addition, future technologies will require integration of biofunctionalized surfaces with microelectronics or micromechanical tools which adds additional complexity (Bousse *et al.* 1983; Linford *et al.* 1995; Strother *et al.* 2000; Yang *et al.* 2002; Buriak 2002*a*,*b*), as most of the microelectronic-compatible materials like silicon, SiO_x and gold show degradation of the biointerfaces in electrolyte solutions (Yang *et al.* 2002).

Diamond can become a promising candidate for bioelectronics as it shows good electronic (Nazare 2001; Nebel & Ristein 2003, 2004; Jackman 2003) and

*Author for correspondence (christoph.nebel@aist.go.jp).

Received 12 October 2006
Accepted 20 November 2006

chemical properties (Angus *et al.* 2004; Swain 2004; Fujishima *et al.* 2005). Figure 1 shows voltammograms for water electrolysis of various electrodes. The supporting electrolyte is 0.5 M H_2SO_4. The graphs are shifted vertically for comparison. Two polycrystalline films, B : PCD(NRL) with 5×10^{19} B cm^{-3} and B : PCD(USU) with 5×10^{20} B cm^{-3} (from Granger *et al.* 1999, 2000), are compared with a single-crystalline boron-doped diamond B : (H)SCD with 3×10^{20} B cm^{-3} and with an undoped diamond (H)SCD (Shin *et al.* 2005). The electrochemical potential window of diamond is significantly larger and the background current within this regime is considerably lower than conventional materials. In addition, by tuning the boron-doping level, the onset of hydrogen evolution (rise of current at negative potentials) can be reduced or switched completely off by decreasing the boron-doping level from extremely high with larger than 10^{20} cm^{-3} boron ('metallic') to 'undoped' (intrinsic diamond). There are also some other parameters affecting the electrochemical potential window like crystal orientation (Kondo *et al.* 2002), structural perfection of polycrystalline diamond (Pleskov *et al.* 1998) and surface termination (Angus *et al.* 2004). Their discussion in this context is, however, beyond the scope of this paper.

Surface-induced conductivity of hydrogen-terminated, undoped diamond in electrolyte solutions is another unique property which has attracted significant attention in recent years (Landstrass & Ravi 1998). It is generated by 'transfer doping' of hydrogen-terminated diamond immersed into the electrolyte solution. The phrase 'transfer doping' indicates that the surface conductivity in diamond arises from missing valence-band electrons as such electrons 'transfer' into the electrolyte (Gi *et al.* 1995; Shirafuji & Sugino 1996; Maier *et al.* 2000). For such transitions, the chemical potential of an electrolyte must be below the energy level of the valence-band maximum. For most semiconductors, this is not the case, as can be seen in figure 2. Even for oxidized diamond, chemical potentials are mostly deep in the bandgap of diamond. It changes drastically if the surface of the diamond, which consists of approximately 2×10^{15} cm^{-2} carbon dangling bonds, is terminated with hydrogen. Hydrogen–carbon bonds are polar covalent bonds (electronegativity of carbon and hydrogen are 2.5 and 2.1, respectively); therefore, a dense surface dipole layer is generated with slightly negative charged carbon (C^-) and slightly positive charged hydrogen (H^+). From basic electrostatics, such a dipole layer causes an electrostatic potential step ΔV perpendicular to the surface over a distance of the order of the C–H bond length of 1.1 Å. Simple calculations show that the energy variation over this dipole is in the range of 1.6 eV (for a detailed discussion see Sque *et al.* 2006). This dipole energy shifts all energy levels of diamond for approximately 1.6 eV up with respect to the chemical potential of an electrolyte (figure 2). Conduction-band states of diamond are now above the vacuum level of the electrolyte and the scenario is called 'negative electron affinity' (see figure 2; clean diamond, where the vacuum level is approx. 0.3 eV above the conduction-band minimum and H-terminated diamond, where the vacuum level is 1.3 eV below the conduction-band minimum; Maier *et al.* 2000; Takeuchi *et al.* 2005). As all electronic states are shifted by the same dipole energy, occupied valence-band states emerge above the chemical potential μ of electrolytes. Electrons from the diamond valence band (electronically occupied states) can therefore tunnel into empty electronic states of the electrolyte until thermodynamic equilibrium between the Fermi level of diamond and the electrochemical potential of the electrolyte is established. This is schematically shown in figure 3*a*. Fermi level and chemical potential, μ, align and form a narrow valence-band bending of 20–30 Å in width, which is in effect a confined hole accumulation layer. Such alignment requires defect-free bulk and surface properties as well as a perfect H-termination.

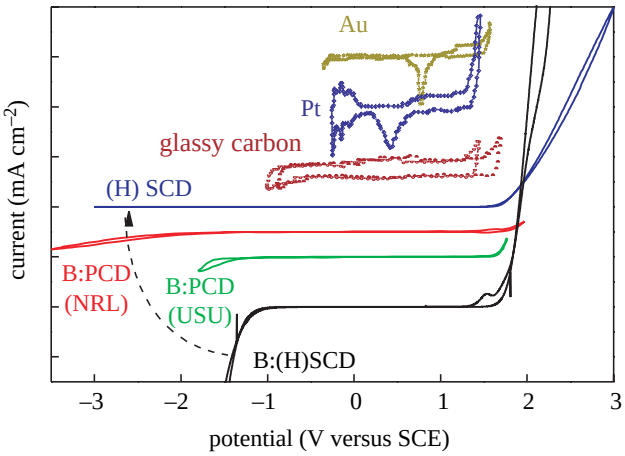

Figure 1. Voltammograms for water electrolysis of various electrodes. The supporting electrolyte is 0.5 M H_2SO_4. The graphs are shifted vertically for comparison. Two polycrystalline films, B : PCD(NRL) with 5×10^{19} B cm^{-3} and B : PCD(USU) with 5×10^{20} B cm^{-3}, from Granger *et al.* (2000) are compared with a single-crystalline boron-doped diamond B: (H)SCD with 3×10^{20} B cm^{-3} and with an undoped diamond (H)SCD. Oxidation reactions, e.g. oxygen evolution, have positive currents and emerge around 1.8 V for all diamond samples. Reduction reactions, e.g. hydrogen evolution, have negative currents and show very different properties.

During recent years, the growth of diamond has been optimized to such a level in combination with a perfect H-termination of the surface (for a review see Nebel *et al.* 2006*c*). As the chemical potential of electrolytes is changing with pH, a variation of the surface conductivity can be predicted and is indeed experimentally detected. It follows closely the Nernst prediction with 55 mV/pH (figure 3*b*; Nebel 2005; Nebel *et al.* 2006*a–c*).

Diamond is known to be biocompatible (Tang *et al.* 1995) and has therefore a potential for *in vivo* electronic applications. When Takahashi *et al.* (2000) first introduced a photochemical chlorination/amination/carboxylation process of the initially H-terminated diamond surface, a giant step towards biofunctionalization of diamond was taken, as the obstacle to 'chemical inertness' of diamond has finally been removed (Takahashi *et al.* 2000, 2003). This triggered more activities so that 2 years later, Yang *et al.* (2002)

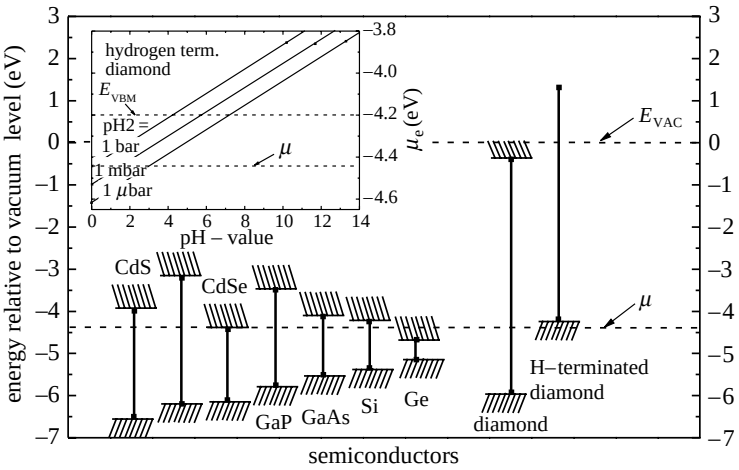

Figure 2. Energies of the band edges of a number of conventional semiconductors and of hydrogenated and hydrogen-free diamond relative to the vacuum level E_{VAC}. The dashed horizontal line marks the chemical potential μ for electrons in an acidic electrolyte under the conditions of standard hydrogen electrode. The insert shows the chemical potential under general non-standard conditions as a function of pH and for different partial pressure of hydrogen in the atmosphere as given by Nernst's equation (Maier *et al.* 2000).

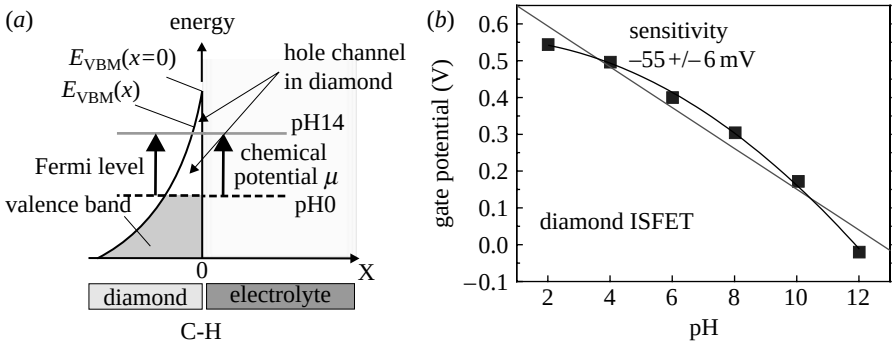

Figure 3. (*a*) Fermi level and chemical potential alignment at the diamond/electrolyte interface after equilibration. Owing to transfer doping, electrons are missing in the diamond and a thin hole accumulation layer is generated. The layer depends on the chemical potential as indicated by arrows. (*b*) pH sensitivity of a diamond ion-sensitive field-effect transistor (ISFET). The gate potential shift shows a pH dependence of 55 mV/pH, which is close to the Nernst prediction.

introduced a new photochemical method to modify nanocrystalline diamond surfaces using alkenes, followed by electrochemical reduction of diazonium salts which has been successfully applied to functionalize boron-doped ultrananocrystalline diamond (Wang *et al.* 2004) and recently, a direct amination of diamond has been introduced (Zhang *et al.* 2006). Such functionalized surfaces have been further modified with DNA, enzymes and proteins, and characterized using fluorescence microscopy (FM) and impedance spectroscopy (Yang *et al.* 2002, 2004; Song *et al.* 2004), voltammetry and gate potential shifts of ion-sensitive field-effect transistors (ISFET; Härtl *et al.* 2004).

Maybe the most influential argument for diamond applications in biotechnology has been given by Yang *et al.* (2002). They characterized the bonding stability of DNA to nanocrystalline diamond and other substrates in hybridization/denaturation cycles using FM investigations. The result is shown in figure 4 in comparison to Au, Si and glassy carbon. It demonstrates that DNA bonding to diamond is significantly better than to other substrates as no degradation of fluorescence intensity could be detected. The long-term

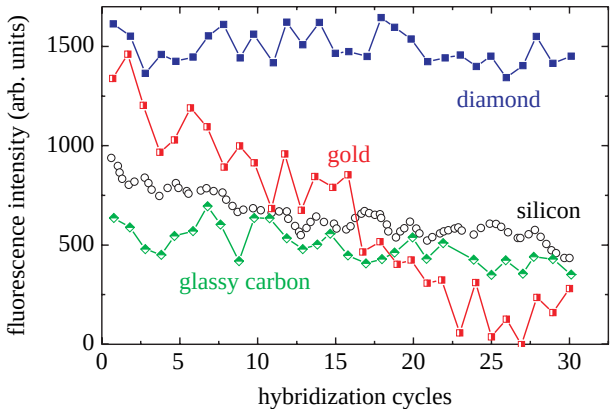

Figure 4. Stability of DNA bonding to ultrananocrystalline diamond and other materials during 30 successive cycles of hybridization and denaturation. In each case, the substrates were amine modified and then linked to thiol-terminated DNA (from Yang *et al.* 2002).

bonding stability is especially important in multiarray sensor applications, which are costly to produce and, therefore, need long-term stability if applied in high-throughput systems.

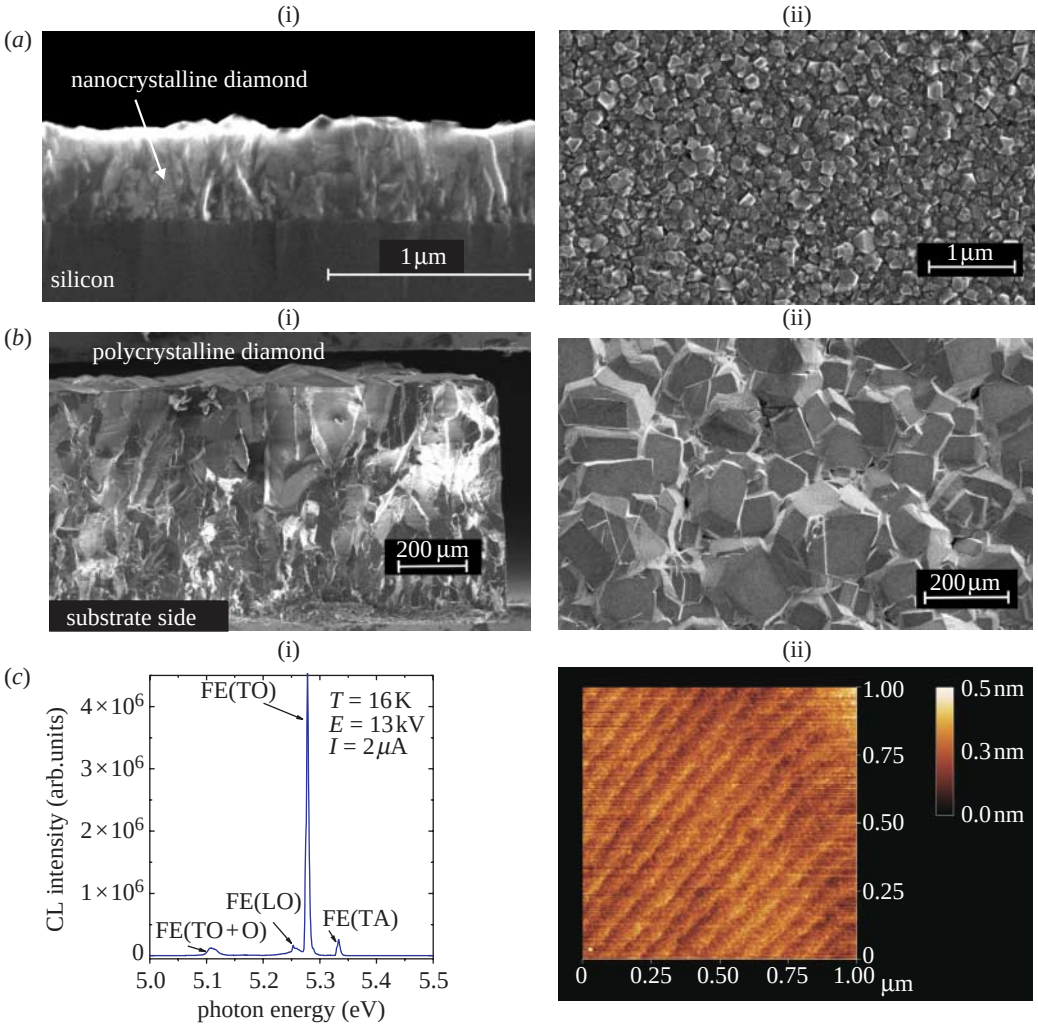

Figure 5. Comparison of different diamond films. (*a*) Nanocrystalline diamond: (i) grain structure; (ii) surface morphology where the typical surface roughness is in the range of 30–50 nm (from O. A. Williams 2006, private communication). (*b*) Polycrystalline diamond: (i) grain structure; (ii) surface morphology with surface roughness of several tens of micrometre. (*c*) Single-crystalline diamond: (i) cathodoluminescence spectrum measured at 16 K; (ii) surface properties as detected with AFM, where atomic steps are detected.

Applications of diamond sensors will ultimately depend on the commercial availability of diamond films. This has improved significantly during recent years as nano- and polycrystalline diamond films can be grown by plasma-enhanced chemical vapour deposition (CVD) heteroepitaxially on silicon and other substrates on a large area. Growth parameters are currently optimized to allow integration into established silicon technology (Carlisle & Auciello 2003; Williams *et al.* 2006; M. Hasegawa 2006, private communication). Single-crystalline diamond, grown by high-temperature, high-pressure growth, is relatively cheap and commercially available owing to the increasing number of companies producing diamond. The size of these substrates is relatively small, typically 4 mm×4 mm which is, however, large enough for homoepitaxial growth of high-quality single-crystalline CVD diamond ('electronic grade quality') on such substrates.

With respect to the electronic applications, a careful selection of 'diamond' material is required. Figure 5 compares structural properties of nano-, poly- and single-crystalline diamond. Ultrananno-, nano- and polycrystalline diamond layers are dominated by grain boundaries which are decorated with sp^2 and amorphous carbon (Nebel 2003*a*,*b*; Nesladek *et al.* 2003). The volume fraction of sp^2 and grain boundaries depends on growth parameter and varies from layer to layer. Especially, ultrananocrystalline diamond contains a relatively high volume fraction of sp^2 of up to 5% (Carlisle & Auciello 2003). Amorphous carbon and sp^2 generate a continuous electronic density-of-states distribution in the gap of diamond. These states will affect sensor's sensitivity and dynamic properties. Therefore, applications of polycrystalline diamond as photo- or high-energy particle detectors show signal drifts ('memory' and 'priming effects') which arise by filling up of grain-boundary states (Bergonzo *et al.* 2003; Bergonzo & Jackman 2004). In addition, such diamond films show a significant surface roughness in the range of 30–50 nm for nanocrystalline diamond and micrometre to tens of micrometres for polycrystalline layers. Commercially available poly-crystalline diamond is therefore often mechanically polished to achieve smooth surfaces. However, this generates a thin, highly damaged diamond surface which deteriorates surface-related electronic applications

as surface defects, approximately 0.9–1.1 eV, above the valence-band maximum pin the Fermi level (Cui *et al.* 1998; Kono *et al.* 2005).

On the other hand, single-crystalline CVD diamond has been optimized over recent years to electronic grade quality with atomically smooth surfaces (figure 5*c*; Takeuchi *et al.* 1999; Watanabe *et al.* 1999; Okushi 2001). Even at room temperature, these films show strong free-excitonic emissions at 5.27 and 5.12 eV, which are fingerprints of a low defect density, typically below 10^{15} cm^{-3}. The bulk resistivity of undoped films at 300 K is larger than 10^{15} Ω cm (Nebel 2003*a*,*b*). Atomic force microscopy (AFM) characterization of such films show surface morphologies which indicate atomically flat properties with step-etch growth, where terraces run parallel to the (110) direction. After H-termination of such layers, heterojunction properties follow very well the predicted properties of defect-free diamond.

The wide-bandgap semiconductor diamond, with a bandgap of 5.47 eV at $T=300$ K, can be doped p-type by boron which results in a doping level of 360 meV above the valence-band maximum (Collins *et al.* 1965). Phosphorus doping has been introduced for n-type doping with the phosphorus doping level of 0.6 eV below the conduction-band minimum (Koizumi *et al.* 1997). Both the levels are basically too deep for room-temperature electronic applications, which is the typical regime of bioelectronics. One way to overcome this problem is the application of metallic doping, where in the case of boron, typically 10^{20} B cm^{-3} or more atoms are incorporated into the diamond (Borst & Weis 1996). This causes enough wave function overlap of holes in acceptor states of boron to realize carrier tunnelling propagate without thermal activation of holes to the valence band. Highly boron-doped diamond is therefore well established in electrochemistry. Applications of n-type diamond in electro- or biochemical sensors seem to be not too favourable, as the Fermi level (0.6 eV below the conduction band) and chemical potential of electrolytes (typically 4.5 eV below the vacuum level, see figure 2) are too different, giving rise to energy-barrier-limited electronic interactions.

This brief introduction of major properties of diamond shows that it is, indeed, an interesting transducer material for biosensor applications. In the following, we review our achievements with respect to interface properties of single-crystalline CVD diamond to organic linker molecular layers and DNA films. We describe surface functionalization using amine and phenyl layers, which are currently attracting significant attention. There are other photochemical modifications of diamond available (e.g. Takahashi *et al.* 2003 or Zhang *et al.* 2006), which are based on direct or indirect surface amination. It is very likely that sooner or later this spectrum will become even broader. We want to focus in the following on amine- and phenyl-related modifications, as these techniques are established, used by a growing number of scientists and characterized reasonably well.

For our experiments, we used homoepitaxially grown, atomically smooth CVD diamonds, either undoped or metallically boron doped, which are free of grain boundaries, sp^2 carbon or other defects. We apply (i) photochemical attachment chemistry of alkene molecules to undoped diamond (Yang *et al.* 2002) and (ii) electrochemical reduction of diazonium salts (Wang *et al.* 2004) to form nitrophenyl linker molecules on boron-doped CVD diamond. The bonding mechanisms, kinetics, molecular arrangements and densities will be introduced using a variety of experiments like X-ray photoelectron spectroscopy (XPS), scanning electron microscopy (SEM), AFM, cyclic voltammetry and several electronic characterization techniques. By using a heterobifunctional cross-linker, the thiol-modified single-stranded probe DNA (ss-DNA) is bonded to the diamond. Such surfaces are exposed to fluorescence-labelled target ss-DNA to investigate hybridization by using FM. We applied AFM in electrolyte solution to gain information about geometrical properties of DNA, bonding strength, as well as the degree of surface coverage. Finally, first we introduced the results with respect to label-free electronic sensing of DNA hybridization using $Fe(CN_6)^{3-/4-}$ redox molecules as mediator in amperometric experiments and variation of gate potential threshold shifts in DNA-FET structures.

2. MATERIALS AND METHODS

2.1. CVD diamond growth, surface modifications and contact deposition

High-quality undoped, single-crystalline diamond films of 200 nm thickness have been grown homoepitaxially on 3 mm×3 mm (100) oriented synthetic diamond substrates, using microwave plasma-assisted CVD. Growth parameters were: substrate temperature 800°C; microwave power 750 W; total gas pressure 25 Torr; total gas flow 400 sccm with 0.025% CH_4 in H_2. Note, the used substrates have been grown commercially by high-pressure, high-temperature techniques and contain typically up to 10^{19} cm^{-3} dispersed nitrogen (type Ib diamond). To achieve H-termination after growth, CH_4 is switched off and the diamond is exposed to a pure hydrogen plasma for 5 min with otherwise identical parameters. After switching off the hydrogen plasma, the diamond layer is cooled down to room temperature in H_2 atmosphere. A detailed discussion on sample growth properties can be found in Takeuchi *et al.* (1999), Watanabe *et al.* (1999) and Okushi (2001).

These films show strong room-temperature free-exciton emission intensities at 5.27 and 5.12 eV (figure 5*c*), which is an indication of low defect densities, typically below 10^{15} cm^{-3}. Layers are highly insulating with resistivities larger than 10^{15} Ω cm. Surfaces are smooth as characterized by AFM. A typical result is shown in figure 6. The root mean square (r.m.s) surface roughness is below 1 Å.

Boron-doped single-crystalline diamond films have been grown homoepitaxially on synthetic (100) Ib diamond substrates with 4 mm×4 mm×0.4 mm size, using microwave plasma-assisted CVD. Growth parameters are: microwave power 1200 W, which generate a substrate temperature around 900°C; gas pressure

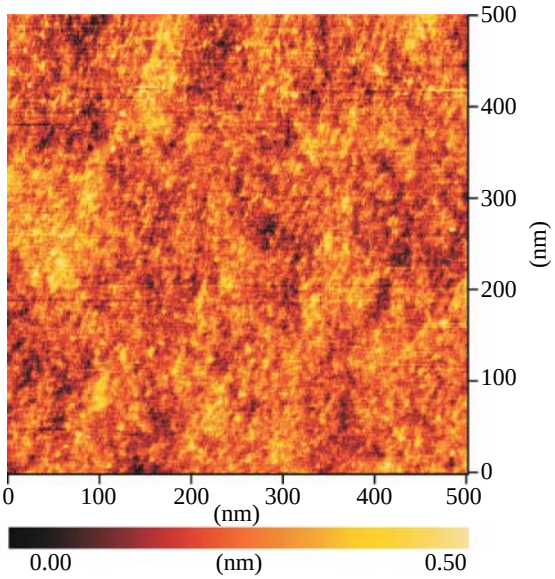

Figure 6. AFM surface morphology of diamond surface used in these studies shows a root mean square (r.m.s.) roughness below 1 Å.

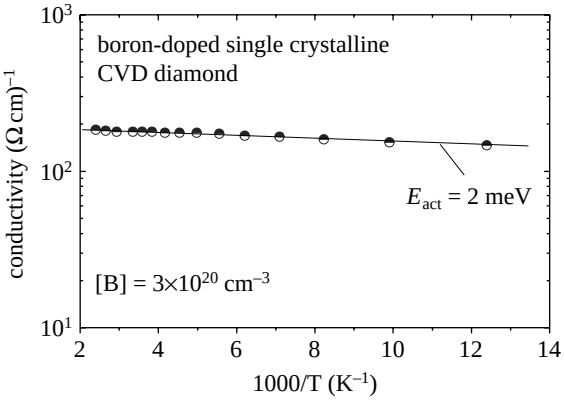

Figure 7. Temperature-dependent conductivity as measured on metallically boron-doped CVD diamond. The doping level is in the range of 5×10^{20} B cm^{-3}. σ is activated with 2 meV, which indicates a hopping process of holes in the acceptor band.

50 Torr; gas flow 400 sccm with 0.6% CH_4 in H_2. B_2H_6, as boron source, is mixed in CH_4, where the boron/carbon atomic ratio (B/C) was 16 000 p.p.m. Typically 1 µm thick films have been grown within 7 h. H-termination has been achieved in the same way as described above. To measure bulk properties, boron-doped diamond is wet-chemically oxidized by boiling in a mixture of H_2SO_4 and HNO_3 (3 : 1) at 230°C for 60 min. Figure 7 shows a typical result of conductivity, σ, which is in the range of 200 $(\Omega\ \mathrm{cm})^{-1}$ at 300 K, showing a negligible activation energy of 2 meV ('metallic properties'). It is achieved by ultra-high doping of diamond with 3×10^{20} cm^{-3} boron acceptors, as detected by secondary ion mass spectroscopy. The crystal quality is not deteriorated by this high boron incorporation. A series of X-ray diffraction (XRD) and Raman experiments have been applied to investigate the details of crystal quality, which will be discussed elsewhere.

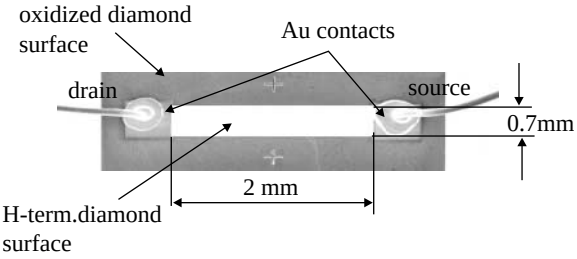

Figure 8. Typical geometry and arrangement of a diamond DNA-FET. The image has been generated by SEM on such a transistor where the sensor area is H-terminated and surrounded by oxidized diamond. Drain and source contacts are Au. The H-terminated area will be photochemically modified to bond ss-DNA marker molecules covalently to diamond.

To obtain patterns of H- and O-termination on diamond surfaces, we apply photolithography, using photoresist as a mask to protect H-terminated areas, while uncovered surface parts are exposed to a 13.56 MHz RF oxygen plasma. Plasma parameters are: oxygen (O_2) gas pressure 20 Torr; plasma power 300 W; and duration 2.5 min. Wetting angle experiments of H-terminated surfaces show angles larger than 94°, indicating strong hydrophobic properties. After plasma oxidation, the wetting angle approaches 0° as the surface becomes hydrophilic.

For electronic characterization or realization of DNA field-effect transistors (DNA-FET), we deposited ohmic contacts on H-terminated diamond by thermal evaporation of 200 nm thick Au onto photoresist-patterned diamond, followed by a lift-off process. In the case of highly boron-doped diamond, Ti (100 Å)/Pt (100 Å)/Au (2000 Å) contacts have been realized using an e-beam evaporation. Figure 8 shows a DNA-FET from diamond as measured by SEM. The sensor area of size 2 mm×0.7 mm is originally H-terminated diamond which connects drain and source Au contacts. This area is surrounded by insulating diamond which has been oxidized. The H-terminated surface is chemically modified as described below to covalently bond DNA to it. For experiments in the electrolyte solution, drain and source contacts are insulated by silicon rubber. We use Pt as gate electrode (not shown) in buffer solutions.

Electrochemical experiments on boron-doped diamond are performed on typical areas of 3 mm^2. Ohmic contacts to boron-doped diamond are evaporated outside of this area and sealed with silicon rubber.

2.2. Photochemical surface modification of undoped diamond

Undoped single-crystalline diamond surfaces are modified by photochemical reactions with 10-amino-dec-1-ene molecules protected with trifluoroacetic acid group (TFAAD; Yang *et al.* 2002). The molecule is shown in figure 9 as determined by molecular orbital calculations. The chemically reactive end is terminated with an olefin (C=C), while the other end is protected from reactions using a trifluoroacetic cap. Chemical

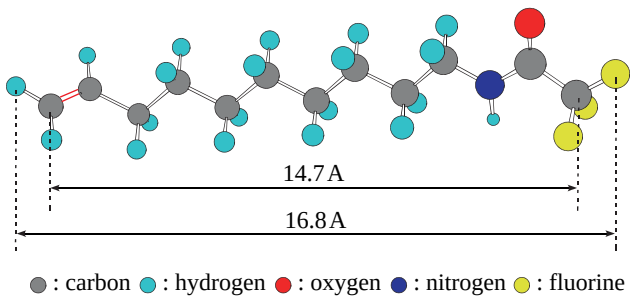

Figure 9. Amino-dec-1-ene molecule protected with trifluoroacetic acid group (TFAAD) as determined by molecular orbital calculations.

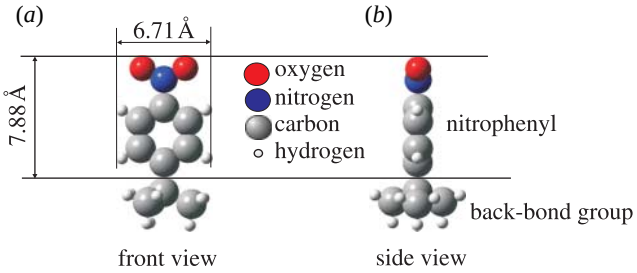

Figure 10. (*a*) Front and (*b*) side view of nitrophenyl molecule as calculated by molecular orbital calculations.

attachment is accomplished by placing 4 µl of TFAAD on the diamond substrate. Then, the TFAAD is homogeneously distributed by spin coating with 4000 rounds/min in air for 20 s, which forms a 5 µm thick liquid TFAAD layer. After accomplishment of spin coating, samples are sealed into a chamber with quartz window in nitrogen atmosphere. Then, UV illumination is switched on for a given period of time. The ultraviolet light is generated in a high-pressure mercury lamp with emission at 250 nm of 10 mW cm^{-2} intensity.

2.3. Electrochemical surface functionalization

Electrochemically induced covalent attachment of nitrophenyl molecules, as introduced by Wang *et al.* (2004), has been performed using an Electrochemical Analyzer 900 (CHI instruments) and a three-electrode configuration with a platinum counter electrode and an Ag/AgCl (0.01 M) reference electrode (BAS, Japan). The active area of the boron-doped diamond working electrode is approximately 0.03 cm^2. Electrolyte solution for the reduction of 4-nitrobenzene diazonium tetrafluoroborate is 0.1 M tetrabutylammonium tetrafluoroborate (NBu_4BF_4) in dehydrated acetonitrile (Wako chemicals; H_2O: less than 50 p.p.m.). The diazonium salts reduction is performed in a N_2-purged glove-box. Nitrophenyl-modified diamond surfaces are then sonicated with acetone and acetonitrile. XPS, AFM and voltammetric experiments have been applied to characterize the surface bonding properties and to reduce the nitrophenyl groups to aminophenyl groups. The nitrophenyl groups grafted on single-crystalline diamond substrate can be considered as covalently bonded free nitrobenzene to diamond as shown in figure 10 (molecular orbital calculations).

2.4. Heterobifunctional cross-linking and DNA attachment

To provide chemically reactive amine groups to the photochemically treated diamond samples, the trifluoroacetamide protecting group was removed by refluxing the TFAAD-modified surface in 2 : 5 MeOH/H_2O with 7% (w/w) K_2CO_3.

The electrochemically modified surfaces of boron-doped diamond with nitrophenyl groups ($–C_6H_5NO_2$) are electrochemically reduced to aminophenyl ($–C_6H_5NH_2$) in 0.1 M KCl solution of EtOH–H_2O to provide reactive aminophenyl groups.

To attach DNA, the amine- or the phenyl layer is then reacted with 14 nM solution of the heterobifunctional cross-linker sulphosuccinimidyl-4-(*N*-maleimidomethyl)cyclohexane-1-carboxylate in 0.1 M triethanolamine (TEA) buffer (pH 7) for 20 min at room temperature in a humid chamber (for details see Yang *et al.* (2002)). The NHS-ester group in this molecule reacts specifically with the $–NH_2$ groups of the linker molecules to form amide bonds. The maleimide moiety was then reacted with 2–4 µl of thiol-modified DNA (300 µM thiol DNA in 0.1 M TEA buffer (pH 7)) by placing the DNA directly onto the surface in a humid chamber and allowed to react for given time between 10 min and 12 h at room temperature. We used the sequence S1 (=5′-HS-C_6H_{12}-T_{15}-GCTTATCGAGC TTTCG-3′) as probe ss-DNA and the sequence F1 (=5′FAM-CGAAAGCTCGATAAGC-3′) as target ss-DNA, where FAM indicates the presence of a fluorescence tag of fluorescein phosphoramidite. To investigate the mismatched interactions, a four-base mismatched target ss-DNA (5′-FAM-CGATTGCTCC TTAAGC-3′) has been used. For some fluorescence experiments, the green label (FAM) has been replaced by red fluorescence markers (Cy5). All the DNA molecules have been purchased from Glen Research (Virginia). A schematic summary of chemical modification schemes is shown in figure 11.

Denaturation of samples has been performed in 8.3 M urea solution for 30 min at 37°C, followed by rinsing in deionized water. Samples are then hybridized again for another DNA cycle.

2.5. X-ray photoelectron spectroscopy, atomic force microscopy and fluorescence microscopy

The chemical attachment is characterized by using a XPS system (Tetra Probe, Thermo VG Scientific) with a monochromatized AlKα source (1486.6 eV) at a base pressure of 10^{-10} Torr. Unless otherwise noted, electrons ejected between 25 and 80° with respect to the surface normal (atomic sensitivity factors: C, 0.296; F, 1; N, 0.477; and O, 0.711) are collected. The mean free path of electrons is assumed to be 36 Å for perpendicular excitation.

Microscopic morphology and structural properties of nitrophenyl and DNA layers have been characterized by atomic force microscopy (AFM; Molecular Imaging PicoPlus). For DNA characterization, layers were immersed into SSPE buffer (300 mM NaCl,

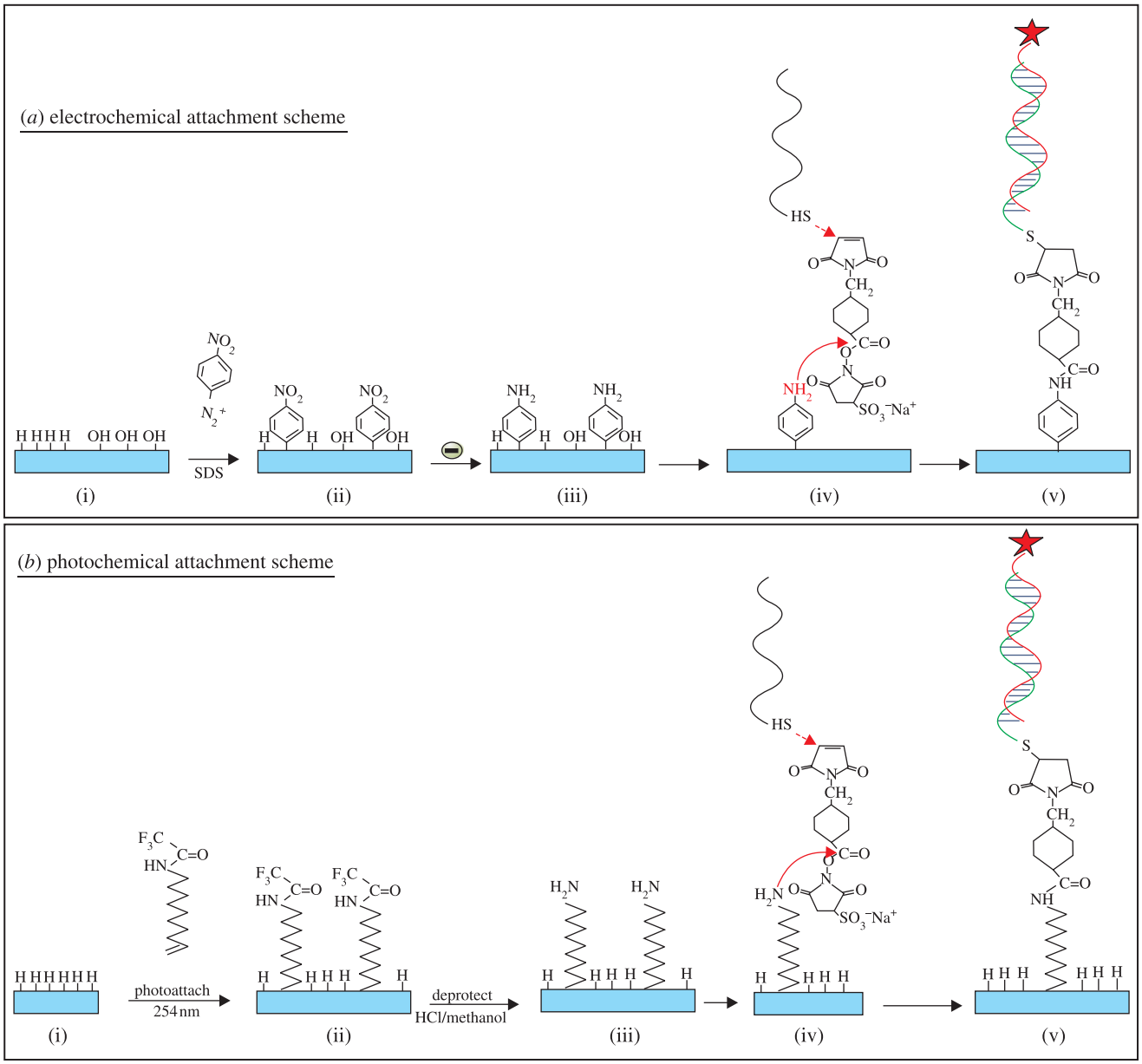

Figure 11. (*a*) Electrochemical and (*b*) photochemical bonding mechanisms. (*a*, i–v) Nitrophenyl linker molecules are electrochemically bonded to H- or O-terminated diamond. Nitrophenyl is reduced to aminophenyl and reacted with a heterobifunctional cross-linker. Finally, thiol-modified ss-DNA is attached. (*b*, i–v) Amine molecules are photochemically and covalently attached to H-terminated diamond. The linker molecules are then deprotected and reacted with the heterobifunctional cross-linker and thiol-modified ss-DNA.

20 mM NaH_2PO_4, 2 mM ethylenediaminetetraacetic acid (EDTA), 6.9 mM sodium dodecyl sulphate (SDS), titrated to pH 7.4 by 2 M NaOH). The buffer solution enables DNA to assume natural conformation and avoids effects of water meniscus around the AFM tip.

Surface morphologies are investigated in oscillating-mode AFM (O-AFM), where the tip–surface interaction is controlled by adjusting the tip oscillating amplitude to a defined value (AFM set-point ratio measurements; Erts *et al.* 2003). The set-point ratio is defined as $r_{SP} = A_O/A_{SP}$, where A_O is the amplitude of free cantilever oscillations and A_{SP} is the amplitude of the tip approaching the surface. Measurements are made typically with A_O of 6 and 10 nm. In addition, we also used cantilever phase shift detection (phase lag of cantilever oscillation with respect to oscillation of the excitation piezo-element) to enhance the material contrast between diamond and DNA.

Molecular bonding properties (mechanical properties) of linker and DNA layers have been characterized by contact mode AFM, where we applied different loading forces to the AFM tip (C-AFM) in the range of 6–200 nN. The scan rate is 10–20 $\mu m\,s^{-1}$. For forces above a critical threshold, linker and DNA molecules are removed. The difference in height is then measured in O-AFM. Doped silicon AFM cantilevers are used in these experiments with a spring constant of 3.5 $N\,m^{-1}$. The cantilever resonance frequency is 75 kHz in air and 30 kHz in buffer solution.

FM has been applied using a Leica Fluorescence Imaging System DM6000B/FW4000TZ, where the fluorescence intensity is evaluated by grey-scale analysis (Leica QWin software). Please note that we

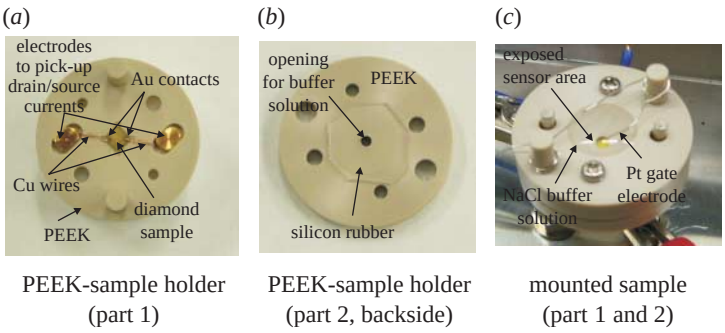

Figure 12. DNA-FET sample holder arrangement. (*a*) The diamond sensor is mounted on a PEEK plate. The drain and source pads are contacted using Cu wire. A second PEEK part (*b*) with silicon rubber is mounted on top of part (*a*) and closed to seal the drain–source pads from electrolyte buffer (*c*). A Pt wire is used as gate electrode and the exposed sensor area is 0.7×1 mm.

have characterized all diamond layers before surface modifications to detect fluorescence emission arising from the bulk of diamond, like, for example, from nitrogen/carbon-vacancy complexes. Samples which showed bulk-flourescence have been excluded from our experiments. The shown fluorescence is, therefore, truly from fluorescence-labelled DNA.

2.6. DNA field-effect transistors

To realize in-plane gate DNA field-effect transistors (DNA-FET), undoped CVD diamonds with atomically smooth surfaces have been grown by microwave plasma-assisted CVD (see above) on Ib substrates. The layer thickness is typically 200 nm. After hydrogen termination of the diamond surface, a H-terminated sensor area of 2 mm×0.7 mm size has been processed by photolithography and plasma oxidation. Two Au contacts (0.7 mm×0.5 mm) evaporated to each end of the H-terminated surface serve as drain and source contacts (figure 8).

Alkene cross-linker molecules are then attached by photochemical means for 12–20 h, followed by the attachment of probe ss-DNA. The density of ss-DNA has been varied between 10^{12} and 10^{13} cm^{-2} for these experiments. Samples are then transferred into polyetheretherketone sample holders as shown in figure 12*a*. Please note that during the transfer, the ss-DNA layer is covered by sodium chloride buffer solution (1 M with 0.1 M phosphate (pH 7.2)). The drain/source contacts are sealed against contact with buffer solution by a silicon rubber (figure 12*b*), which is also used to press copper wires to the drain and source Au contacts (figure 12*a*). A top view of the set-up is shown in figure 12*c*. The PEEK top part has been designed in a way such that 1 mm of the sensor area is exposed to buffer solution. To apply well-defined gate potentials, we use a thin Pt wire of 0.2 mm diameter, which is immersed into the sodium chloride buffer. Drain–source currents are measured as a function of gate potential that has been varied between 0 and −0.6 V. The gate threshold potential of DNA-FETs has been characterized by applying several cycles, where properties of the FET with probe ss-DNA have been determined first, followed by determination of FET properties after hybridization with complementary target ss-DNA. Then, the sample has been denatured and characterized again.

3. RESULTS

3.1. Photochemical surface modifications of undoped single-crystalline diamond

The H-terminated samples are photochemically reacted with long-chain ω-unsaturated amine, 10-aminodec-1-ene, that has been protected with the trifluoroacetamide functional group (Nebel *et al.* 2006*d*,*e*). We refer to this protected amine as TFAAD. A variety of attachment experiments on H-terminated and oxidized diamond surfaces show that this process works only on H-terminated diamond. Figure 13*a* shows the XPS survey spectra of a clean hydrogen-terminated single-crystalline diamond surface before and after exposed to TFAAD and 10 mW cm^{-2} UV illumination intensity (254 nm) for 2 h. Before XPS measurements, samples were rinsed in chloroform and methanol (each 5 min in ultrasonic). The overall spectrum shows a strong fluorine peak with a binding energy of 689 eV, an O(1s) peak at 531 eV, a N(1s) peak at 400 eV and a large C(1s) bulk peak at 284.5 eV. Please note that on clean H-terminated diamond only the C(1s) peak at 284.5 eV can be detected. After photoattachment, the C(1s) spectrum reveals two additional small peaks at 292.9 and 288.5 eV (figure 13*b*), which are attributed to carbon atoms in the CF_3 cap group and in the C=O group, respectively. From these experiments, we conclude that UV light of approximately 250 nm (5 eV) initiates the attachment of TFAAD to H-terminated single-crystalline diamond. The ratio of the F(1s) XPS signal (peak area) to that of the total C(1s) signal (R_{FC}) as a function of illumination time is shown in figure 13*c*. The time dependency of R_{FC} follows approximately an exponential law, $R_{FC} = A\{1-\exp(-t/\tau)\}$, with a characteristic time constant τ of 1.7 h. Saturation of the area ratio F(1s)/C(1s) is achieved after approximately 7 h.

Angle-resolved XPS experiments shown in figure 13*d* are used to calculate the density of TFAAD molecules bonded to diamond in absolute units. As parameters, we used the following data: density of carbon atoms = 1.77×10^{23} atoms cm^{-3}; atomic sensitivity factors of C (0.296) and F (1); and a mean free path for perpendicular illumination = 36.7 Å. Taking into account the area ratio F(1s)/C(1s) results in approximately 2×10^{15} cm^{-2} TFAAD molecules bonded after 7 h. This corresponds to the formation of a monolayer TFAAD as the surface density of carbon bonds on diamond is

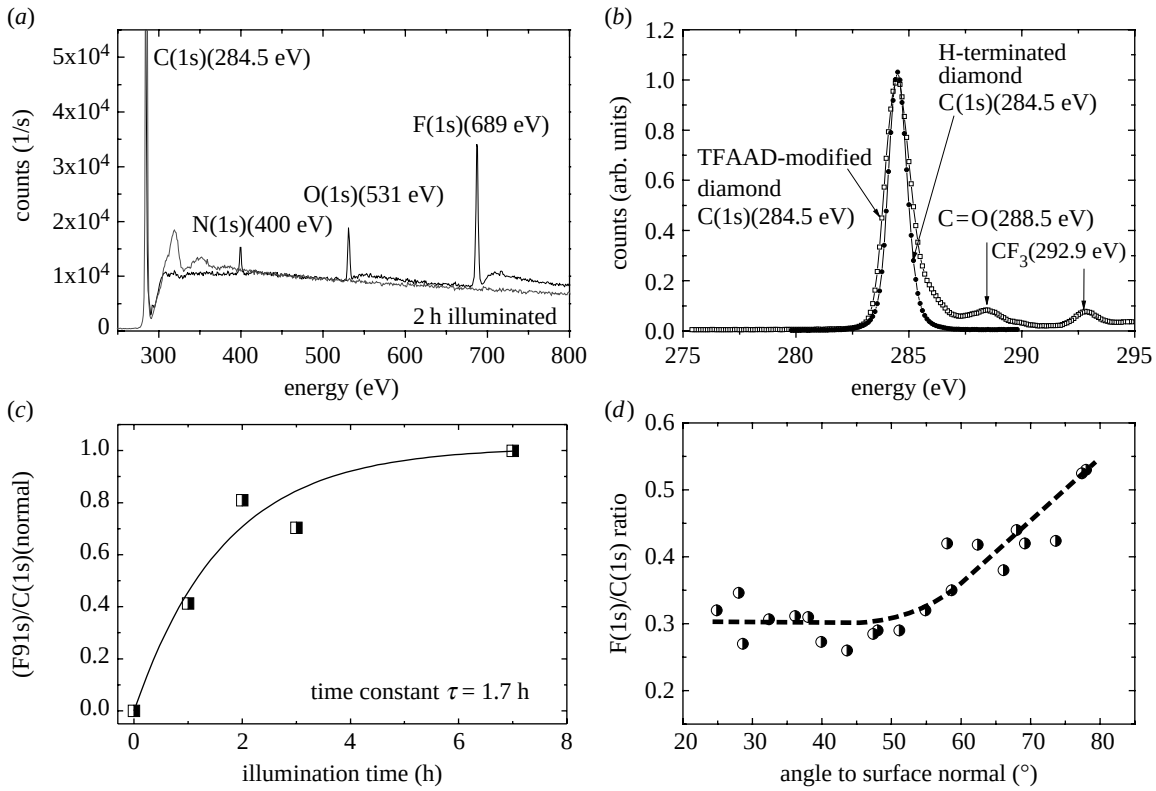

Figure 13. (*a*) XPS survey spectrum of a hydrogen-terminated single-crystalline diamond surface that was exposed to TFAAD and 20 mW cm^{-2} UV illumination (250 nm) for 2 h. (*b*) The C(1s) spectrum reveals two additional small peaks at 292.9 and 288.5 eV, which are attributed to carbon atoms in the CF_3 cap group and in the C=O group, respectively. (*c*) The ratio of the F(1s) signal (peak area) to that of the total C(1s) signal as a function of illumination time is time dependent and follows an exponential increase (dashed line), with a characteristic time constant τ of 1.7 h. (*d*) Angle-resolved (with respect to the surface normal) XPS experiments show an increase in the F(1s)/C(1s) peak intensities, rising from 48 to 78°.

1.5×10^{15} cm^{-2}. However, the TFAAD layer itself consists of 12 carbon atoms which contribute to the signal, so that the real coverage is smaller than this number. Nichols *et al.* (2005) calculated from XPS experiments a layer density of approximately 2×10^{14} TFAAD molecules cm^{-2}, by taking into account both, the bulk and the attached molecules. This is supported by our experiments on single-crystalline diamond in SSPE buffer solution (300 mM NaCl, 20 mM NaH2PO4, 2 mM EDTA, 6.9 mM SDS, titrated to pH 7.4 by 2 M NaOH) before (100% H-termination) and after TFAAD attachment. A typical result is shown in figure 14. A perfectly H-terminated diamond gives rise to a drain–source current of approximately 7.5 µA at $U_G=-0.6$ V. After photoattachment of TFAAD molecules for 20 h, the drain–source current decreased to 3 µA, which is 40% of the initial drain–source conductivity. In the case of 100% H-removal by photoattachment, the drain–source conductivity would completely disappear. We therefore assume that the highest packing density of TFAAD molecules on diamond is, indeed, in the range of approximately 10% or similar to 2×10^{14} cm^{-2} (Nichols *et al.* 2005). Quantum efficiency calculations of the bonding process show that only one electron out of 1600 gives rise to TFAAD bonding (Nebel *et al.* 2006*d*,*e*).

Angle-resolved XPS experiments also give some insight into the geometrical properties of TFAAD molecules on diamond (Hamers *et al.* 2005). Electrons ejected by fluorine and carbon in a random film have

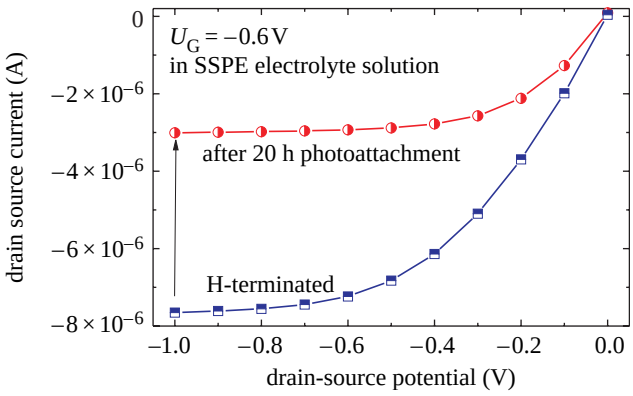

Figure 14. Comparison of diamond ion-sensitive field-effect transistor properties (ISFET) measured in SSPE buffer with perfect H-termination of the surface (squares) and after photoattachment for 20 h (circles).

nearly equal trajectories through the film, so that F(1s) photoelectrons form CF_3 cap groups and C(1s) photoelectrons will undergo similar amounts of inelastic scattering within the film. However, in the case of an oriented film with CF_3 groups at the top, one expects that the C(1s) intensity will be scattered more effectively and the F(1s)/C(1s) ratio observed by XPS will increase. Figure 13*d* shows the results as a function of angle with respect to the surface normal. As the angle is increased from 48 to 78°, the measured F/C intensity ratio increases. It demonstrates that the photochemical modification of H-terminated single-crystalline

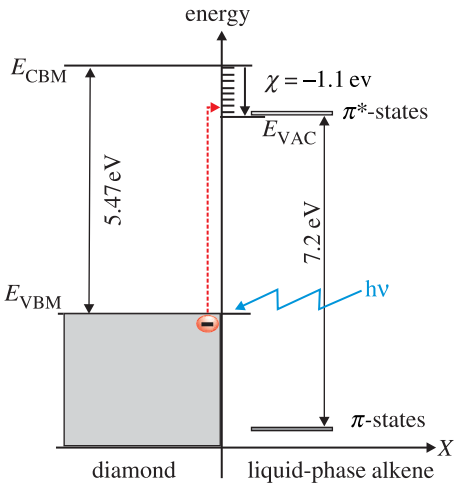

Figure 15. Photoexcitation mechanism at the surface of diamond in contact with TFAAD. Valence-band electrons are photoexcited into empty surface states of diamond and then into empty states of TFAAD molecules which generates nucleophilic properties.

diamond produces oriented molecular layers of TFAAD with the protected amine group at the exposed surface, where it is accessible to further reactions. This is in good agreement with data reported in the literature for nanocrystalline diamond (Hamers *et al.* 2005; Nichols *et al.* 2005). Please note that for angles smaller than 45°, the ratio is nearly constant. We attribute this to the fact that below 45°, the variation in effective scattering thickness is weakly changing, whereas above 45°, the scattering thickness rises strongly (approx. $1/\cos(\alpha)$).

Detailed *in situ* characterization of the attachment process indicates that electron emission by sub-bandgap light triggers the covalent bonding of TFAAD molecules to diamond (Nichols *et al.* 2005; Nebel *et al.* 2006*d*,*e*). In this process, valence-band electrons are optically excited into empty hydrogen-induced states, slightly above the vacuum level as shown schematically in figure 15 (Sque *et al.* 2006). From there, they can reach unoccupied π^* states of TFAAD molecules, generating a nucleophilic situation in the C=C bonding structure. Unfortunately, details about the atomic bonding mechanism of TFAAD to diamond are still not revealed. Two probable scenarios have been introduced (Nichols *et al.* 2005). One is the formation of alkene anions which then react directly with hydrogen bonded to carbon at the diamond surface. The other is the formation of anions that abstract H atoms from the surface, thereby creating carbon surface dangling bonds that covalently bond to other alkene molecules in the liquid. Surface dangling bonds seem to be reactive towards alkenes as demonstrated by Cicero *et al.* (2002). Further experiments are clearly required to gain better insight into this complex process.

3.2. DNA bonding and geometrical properties

To attach DNA, we applied the recipe introduced by Yang *et al.* (2002) and Hamers *et al.* (2005), where the protected amine is first deprotected, leaving behind a primary amine. The primary amine is then reacted with the heterobifunctional cross-linker sulphosuccinimidyl-4-(*N*-maleimidomethyl)cyclohexane-1-carboxylate and finally with thiol-modified DNA to produce the DNA-modified diamond surface. In our experiments, we used a 4 µl droplet which is placed on the diamond layer and covers a circular area of approximately 2 mm in diameter, thereby covering oxidized and H-terminated surface parts. To assess whether DNA-modified diamond surfaces have been generated, such surfaces have been exposed to complementary oligonucleotides that were labelled with fluorescence tags FAM6. Figure 16 shows the result of intense green fluorescence (equal to 100%) from originally H-terminated regions and less intense fluorescence (approximately equal to 70%) from oxidized surface areas, respectively. The weak fluorescence contrast between the two has two reasons. The first reason is that non-covalently bonded DNA is attached to oxidized diamond. This will be discussed in §3.3 using AFM experiments. The other reason is that transparent diamond gives rise to light trapping, so that the transparent diamond appears green in the case of fluorescence emission.

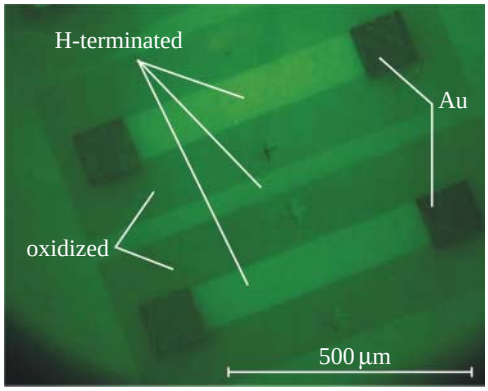

Figure 16. Fluorescence microscopy (FM) image of hybridized DNA on diamond using green fluorescence tag for the complementary DNA. The bright areas are initially H-terminated and the less intense regions were originally oxidized. Black areas are Au contacts.

3.3. Atomic force microscopy (AFM) of DNA on single-crystalline diamond

DNA-functionalized and hybridized surfaces are characterized by AFM measurements in 2×SSPE/0.2% SDS buffer solution (Rezek *et al.* 2006). By performing contact mode AFM (C-AFM) scratching experiments, DNA can be removed and at the interface between clean and DNA-covered diamond, the height of DNA has been measured. In addition, the force required to penetrate and remove DNA has been determined, giving insight into the mechanical stability of the bonding. Scratching experiments were performed with different tip loading forces between 10 and 60 nN as shown in figure 17*a*. For each force, an area of 2 µm×10 µm has been scratched (scan rate: 20 µm s^{-1}). Forces around 45 nN (±12 nN) generate a 100% clean area, which appears darker in fluorescence microscopy FM images as shown in figure 17*b*.

C-AFM experiments on the boundary between initially oxidized and H-terminated diamond are

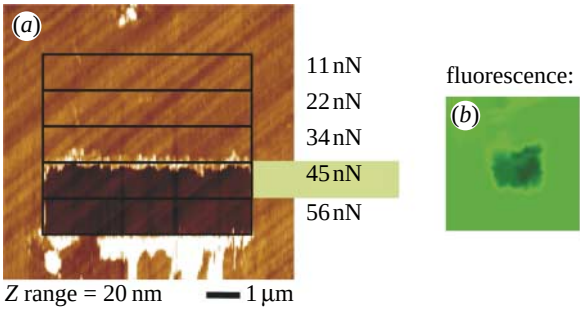

Figure 17. (*a*) Contact mode AFM is shown which gives rise to DNA removal if the force exceeds 45 nN on photochemically treated and initially H-terminated diamond. (*b*) After removal of DNA from the surface, it appears dark in fluorescence microscopy (FM).

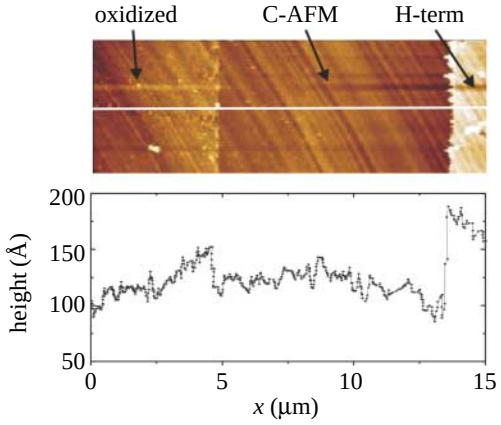

Figure 18. Oscillatory AFM measurements applied at the boundary of cleaned diamond surface to (left) initially oxidized and (right) initially H-terminated diamond show that DNA molecules are present on both the areas. The height on O-terminated diamond is, however, lower than on H-terminated diamond. Molecules on oxidized diamond can be removed with forces of approximately 5 nN.

shown in figure 18. With C-AFM, we detect non-covalently bonded DNA on oxidized diamond. These molecules can be removed with forces around 5 nN. This is five times lower than for DNA bonded to the H-terminated surface. The layer is also significantly thinner as on the H-terminated diamond.

By measuring across the boundary between the DNA-functionalized and the cleaned surface, using oscillatory or tapping mode (O-AFM), the DNA layer thickness can be obtained as shown in figure 19. O-AFM is preferable to C-AFM on soft layers as the tip–surface interaction can be minimized by monitoring the phase shift of the cantilever oscillations (Erts *et al.* 2003). The phase shift was measured as a function of the set-point ratio, $r_{sp} = A_o/A_{sp}$, where A_{sp} is the set-point amplitude and A_o is the amplitude of free cantilever oscillation, on DNA-functionalized and cleaned diamond surface regions (see squares in figure 19*a*). Figure 20 summarizes the results of phase contrast and set-point ratio measurements. The phase contrast between diamond and DNA is positive and approaches zero for set-point ratios approaching 1, i.e. for increasing tip–surface distance. For a phase contrast near 0, which corresponds

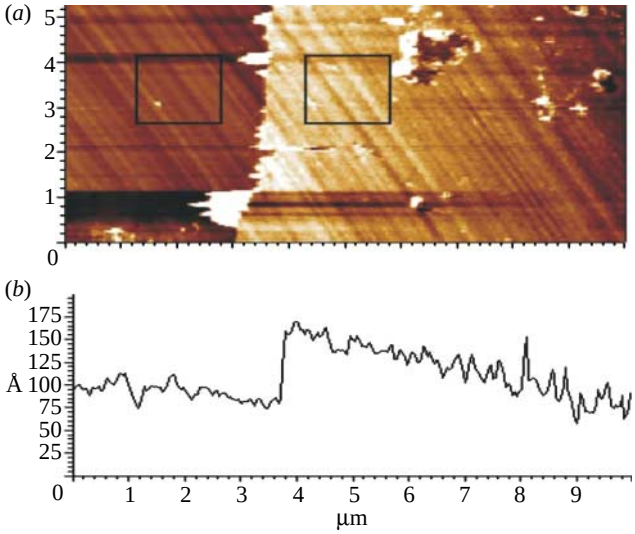

Figure 19. (*a*) Optimized oscillatory AFM measurement at the boundary of cleaned diamond surface and double-stranded DNA molecules bonded to single-crystalline diamond. The squares denote the regions where AFM phase shifts were evaluated. (*b*) AFM height profile across the boundary reveals a DNA layer thickness of 76 Å.

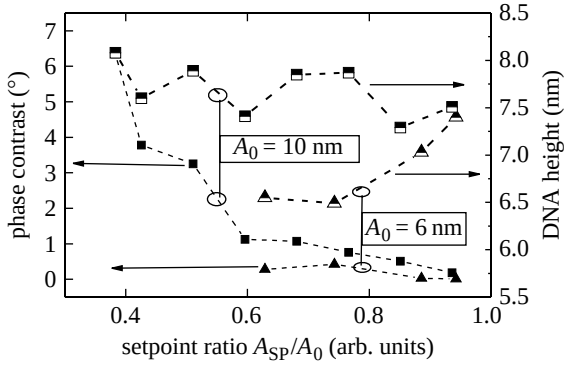

Figure 20. AFM set-point ratio dependence of AFM measurements of DNA height and phase contrast across DNA-functionalized and cleaned diamond surface for free oscillation amplitudes (A_0) of 6 and 10 nm. Extrapolation to set-point ratio 1 results in a DNA height of approximately 76 Å.

to minimized tip–surface interaction, the DNA layer thickness reaches approximately 75–78 Å. Simple O-AFM measurements result in approximately 70 Å (figure 19), which is slightly smaller than the real DNA thickness. The height of 75–78 Å is, however, still significantly lower than the expected height of approximately 130 Å for upright standing DNA (105 Å) on linker (12 Å) and cross-linker molecules (6 Å) and fluorescence marker FAM6 (5 Å). We attribute this to a tilted arrangement of DNA molecules as shown in figure 21. Using triangular geometry, the tilt angle is around 33–36°, which is similar to results of DNA bonded to gold (Erts *et al.* 2003).

A topographic surface profile of DNA double helix molecules bonded on diamond is shown in figure 22. It reveals broad undulations due to the collective interaction of several DNA oligomers with the tip. The height is modulated periodically with an amplitude

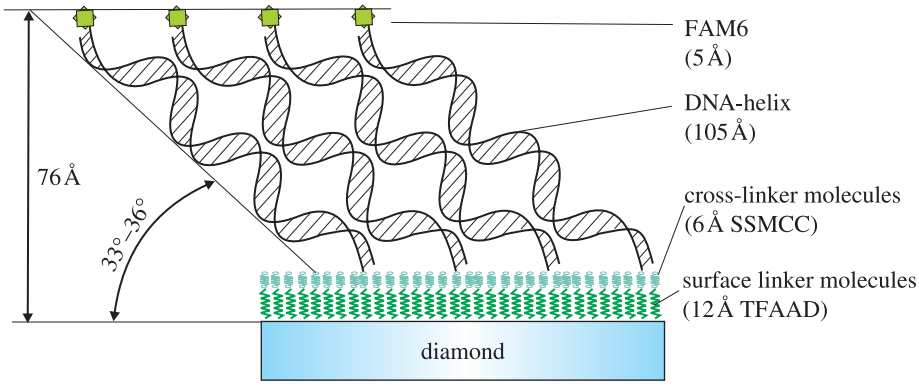

Figure 21. Compact DNA layers of 76 Å height are resolved by optimizing phase and height contrast in AFM. The axis of double helix DNA is therefore tilted at approximately 30–36° with respect to the diamond surface.

around ±5 Å. No pinholes can be detected in the layer. Obviously, a closed DNA film has been synthesized on diamond using photochemical attachment.

For sensor applications, dilute DNA films in the range of 10^{12}–10^{13} cm^{-2} are required (Poghossian *et al.* 2005). To decrease the bonding density we reduce the time of marker DNA attachment. A saturated and very dense film is achieved after 12 h exposure. Following the arguments of Takahashi *et al.* (2003), this will result in a DNA density of approximately 10^{13} cm^{-2}. By decreasing the time of marker ss-DNA attachment, the density can be decreased to 10^{12} cm^{-2} as shown in figure 23. Here, we have evaluated the change in fluorescence intensity after hybridization, where the attachment of ss-DNA marker molecules has been varied between 10 min and 12 h. The attachment kinetics are well described empirically by an exponential function with a time constant, τ, of approximately 2 h.

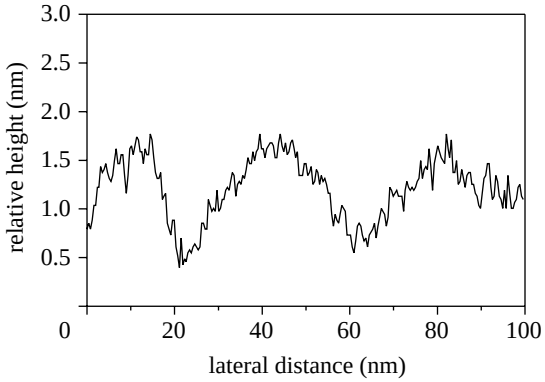

Figure 22. AFM height profile shows a dense DNA layer with r.m.s. height modulations of ±5 Å.

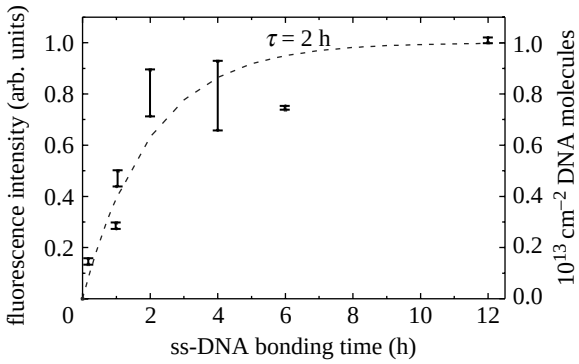

Figure 23. Variations in ss-DNA marker molecule attachment time has been applied between 10 min and 12 h. The fluorescence intensity of hybridized DNA follows an activated property with a time constant of 2 h. Therefore, the DNA density on diamond should vary between 10^{12} and 10^{13} cm^{-2}.

3.4. Electrochemical surface modifications of boron-doped single-crystalline diamond

In the following, we summarize the electrochemical modification of highly conductive p-type single-crystalline CVD diamond (Shin *et al.* 2006). The general chemical scheme is shown in figure 11*a*, where hydrogen-terminated or oxidized diamond is modified with phenyl molecules (step (i) to (ii)). Figure 24 shows cyclic voltammograms of 4-nitrobenzene diazonium salts (1 mM) reactions on highly B-doped single-crystalline CVD diamond film in 0.1 M NBu_4BF_4 acetonitrile solution (scan rate: 0.2 V s^{-1}). An irreversible cathodic peak of the first sweep at −0.17 V (versus Ag/AgCl) indicates nitrophenyl group attachment by diazonium salt reduction (Wang *et al.* 2004). The reduction peak on single-crystalline diamond films decreases rapidly with increasing number of scans within +0.5 to −1.0 V (versus Ag/AgCl), owing to the increasing surface passivation with nitrophenyl molecules.

The electrochemical attachment works not only on the H-terminated diamond, but also on the oxidized diamond surfaces. The voltammetric peak is shifted from −0.17 V for H-termination to −0.41 V (versus Ag/AgCl) for oxidized diamond. This potential shift of $\Delta U = 240$ mV arises by a change in heterojunction properties at the solid/liquid interface. H-terminated diamond has a negative electron affinity around −1.1 eV, while oxidized diamond shows positive affinities (Cui *et al.* 1998; Takeuchi *et al.* 2005). Higher potentials are therefore required for oxidized than for H-terminated diamond to achieve electron transfer. Details of bonding to oxidized diamond are currently under investigation and have to take into account also carbon–oxygen and carbon–carbon bonding arrangements and bond-breaking mechanisms.

After electrochemical derivatization, the diamond substrates are sonicated in acetonitrile, acetone and isopropanol, in order to investigate the properties of

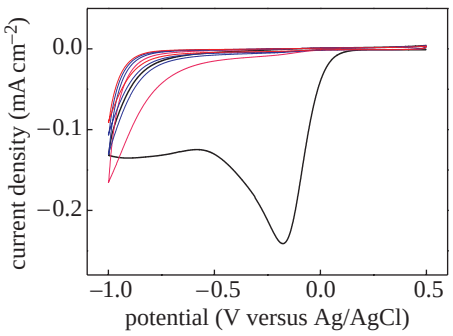

Figure 24. Cyclic voltammograms for 1 mM 4-nitrobenzene diazonium tetrafluoroborate on highly B-doped single-crystalline diamond (DRC). Electrolyte solution: 0.1 M NBu_4BF_4 in CH_3CN; scan rate: 0.2 V s^{-1}.

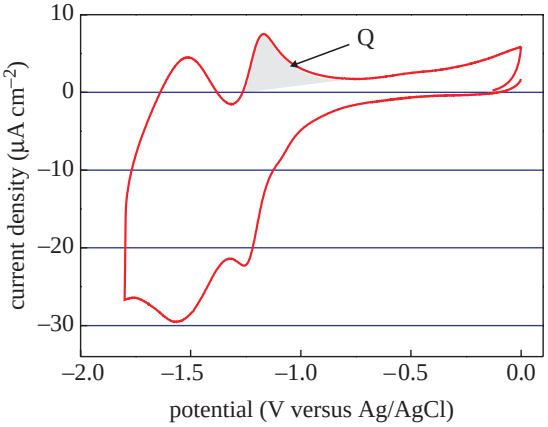

Figure 25. Cyclic voltammograms from 4-nitrophenyl-modified single-crystalline diamond in blank electrolyte solution. Electrolyte solution: 0.1 M NBu_4BF_4 in CH_3CN.

attached nitrophenyl layers in 0.1 M NBu_4BF_4 solution. Nitrophenyl groups grafted on single-crystalline diamond films show two reversible electron-transfer steps, which are reproducibly detected in all potential sweeps (figure 25). The generalized reversible redox reactions of this system are summarized in figure 26. To estimate the surface coverage (Γ) of nitrophenyl groups on diamond, we use the transferred charge of the electron-transfer reaction at −1.17 V (see shaded area in figure 25). This results in 3.8×10^{-7} C cm^{-2} or 8×10^{13} molecules cm^{-2}, indicating the formation of a sub-monolayer on diamond (5% coverage; Shin *et al.* 2006).

Detailed investigations of phenyl layer formation on other electrodes show that this simple interpretation is misleading (Allongue *et al.* 2003; Pinson & Podvorica 2005). In most cases, multilayers are deposited. We have therefore applied additional experiments to characterize the growth and thickness of the phenyl layer on diamond. Generally, all performed contact- and oscillatory-mode AFM experiments on deposited nitrophenyl layers reveal layer thicknesses in the range of 28–68 Å. Taking into account the length of nitrophenyl molecules of approximately 8 Å (figure 10), they indicate clearly multilayer formation by cyclic voltammetry deposition.

A better controlled growth of phenyl films on diamond can be achieved by electrochemical means, applying fixed potentials for a given period of time instead of potential cycles (Allongue *et al.* 2003). In our case, we applied −0.2 V (versus Ag/AgCl) and measured the transient current during the deposition. The result is shown in figure 27. In the case of unlimited electron transfer and diffusion-limited attachment, the dynamics follow the Cottrell law ($i(t)\approx t^{-0.5}$) as introduced by Allongue *et al.* (2003). At the very beginning of the transient current such a characteristic can be detected. However, for longer times, the current decays faster than predicted by this law. We assume that the growing phenyl layer limits an effective electron transfer, slowing down the bonding process. The density of electrons involved in this reaction saturates around 4×10^{15} cm^{-2}.

To verify the layer formation, contact mode AFM has been applied. With increasing force to the tip, the phenyl layer can be removed from diamond. A typical result is shown in figure 28, where the nitrophenyl layer has been attached by one cyclic voltammetry scan (from +0.5 to −1.0 V versus Ag/AgCl at a scan rate of 200 mV s^{-1}). Forces below 100 nN do not damage the phenyl film. Above 100 nN, a layer of 26 Å thickness is removed and forces above 120 nN give rise to the removal of a thin layer, 8 Å in thickness. We assume that a random-oriented phenyl layer is removed first, while forces above 120 nN are required to remove phenyl linker molecules bonded to the diamond.

AFM characterization on phenyl layers, which have been grown at a constant potential of −0.2 V for different times, indicates three-dimensional growth as shown in figure 29 (applied tip force: 200 nN; scan rate: 4 μm s^{-1}). After short-time attachment (5 s), the thickness of the layer is already between 8 and 23 Å. The thickness variation decreases with increasing attachment time, saturating around 25 Å. Taking into account the saturated electron density of 4×10^{15} cm^{-2} and the final thickness of the phenyl layer of 25 Å, the phenyl molecule density in the layer is approximately 2×10^{21} cm^{-3}.

The orientation of phenyl molecules has been characterized by angle-resolved XPS experiments. The integrated peak intensities of O(1s) to C(1s) show a strong angle dependence for attachments at −0.2 V for times up to 40 s (figure 30). We attribute this to an oriented growth of nitrophenyl, with NO_2 molecules preferentially located on the growing top of the layer. This is different in case of much thicker layers (30–65 Å), attached by five cycles in the range of +0.5 to −1.0 V versus Ag/AgCl at a scan rate of 200 mV s^{-1}. Here, the XPS angle variation is weak and the molecules are arranged in a more disordered structure.

From these experiments we conclude that the formation of phenyl layers on diamond is governed by three-dimensional growth, with preferential alignment of NO_2 cap molecules on the top of the growing films, if films are not growing too thick. Growth saturates at a layer thickness of approximately 25 Å, using constant potential attachment (−0.2 V), while significantly thicker layers in the range of 35–65 Å are detected after cyclic attachment (+0.5 to −1 V). Properties of such thick layers are governed by a more random molecule orientation.

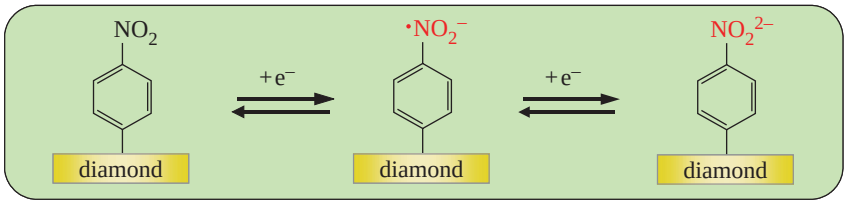

Figure 26. Schematic reduction/oxidation reactions of nitrophenyl bonded to diamond giving rise to a two-electron transfer reaction mechanism.

Subsequently, nitrophenyl groups are electrochemically reduced to aminophenyl ($-C_6H_5NH_2$) in 0.1 M KCl solution of EtOH–H_2O solvent (figure 31). The first voltammetry sweep gives rise to an irreversible reduction peak at −0.94 (versus SCE), which is not detected in the second and higher cyclic voltammetry cycles. Such modified surfaces are then used for chemical bonding to heterobifunctional cross-linker molecules, SSMCC and thiol-modified probe DNA oligonucleotides.

Figure 32 shows a fluorescence image of ss-DNA (S1) marker molecules bonded to diamond after hybridization with its complementary ss-DNA target molecules (F1) labelled with Cy5. The image shows DNA bonding to initially H-terminated diamond and to oxidized diamond. The laid 'T'-shape pattern in figure 32 arises from surface oxidation. The fluorescence from this area is approximately 10% weaker than from hydrogen-terminated diamond. As the light intensity is proportional to the density of fluorescence centres, the density of DNA bonded to oxidized diamond is approximately 10% smaller than on H-terminated diamond. No fluorescence can be detected using a four-base mismatched ss-DNA target molecule for hybridization.

3.5. *Atomic force characterization of DNA bonded electrochemically to boron-doped single-crystalline diamond*

Geometrical properties as well as density and bonding strength of DNA bonded by electrochemical technique to boron-doped diamond has been characterized by AFM experiments as described in §§2.5 and 3.3.

The height of DNA layers is detected to be around 90 Å. This is slightly higher than in the case of photoattachment and arises from the thicker linker molecule layer, which is approximately 25 and 12 Å for the phenyl and the amine linkers, respectively. Again, a tilted arrangement is deduced, comparable to results from photoattachment (approx. 35°). The layer is dense with no pinholes. The removal forces are between 60 and 122 nN, the statistical average around 76 nN. It is interesting to note that on initially oxidized diamond, the forces are lower, namely in the range of 34 nN. A comparison of forces is shown in figure 33. These results indicate strong bonding of DNA to diamond for both, the photo- and the electrochemical surface modifications. Removal forces are about two times higher than that detected on Au and mica as summarized in figure 34 (Xu *et al.* 1999; Schwartz 2001; Zhou *et al.* 2002; Crampton *et al.* 2005). This is promising with respect to diamond biosensor applications where exceptional chemical stability is required.

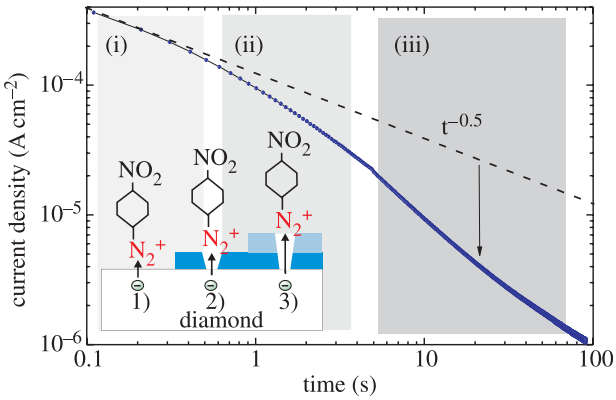

Figure 27. Transient current as detected during nitrophenyl attachment at a constant potential of −0.2 V (versus Ag/AgCl). Also shown is the theoretical decay following a $t^{-0.5}$ time dependence.

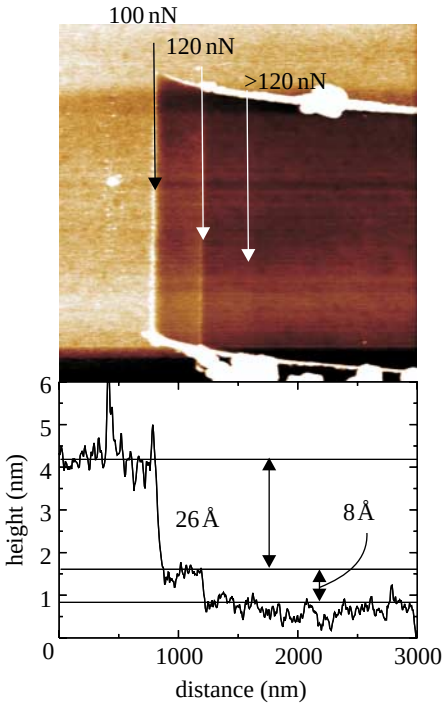

Figure 28. AFM scratching experiments on nitrophenyl-modified diamond. With forces above 100 nN, most of the phenyl layers can be removed, while forces above 120 nN are required to remove the linker layer from the diamond.

3.6. *Electronic detection of DNA hybridization*

Most of the DNA detection techniques are based on DNA hybridization events. In DNA hybridization, the target ss-DNA is identified by a probe ss-DNA that gives rise to hybridization. This reaction is known to be

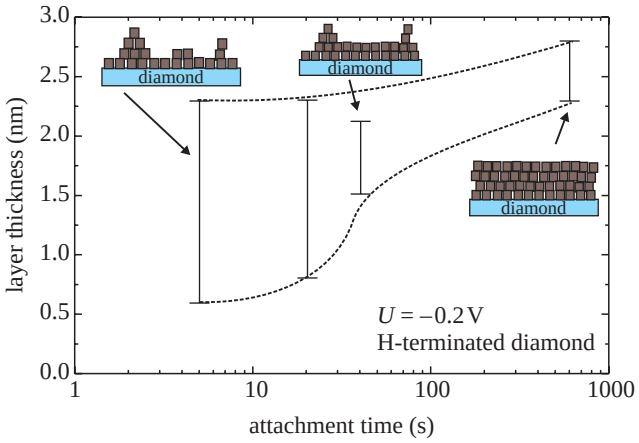

Figure 29. The nitrophenyl layer growth during constant potential attachment experiments with −0.2 V (versus Ag/AgCl) in a three-dimensional fashion. After short-time attachment, the layer thickness varies strongly, whereas after 90 s, the variations become much smaller, indicating a saturated thickness of approximately 25 Å.

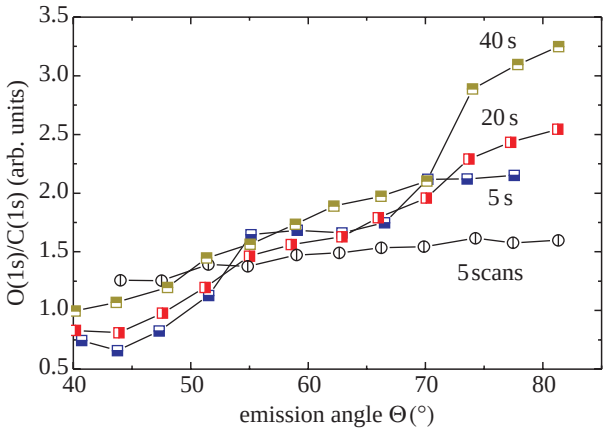

Figure 30. Angle-resolved XPS experiments show oriented growth of layers grown with constant potential. Cyclic attachment gives rise to significantly thicker layers of typically 30–70 Å with less pronounced molecule arrangement.

highly efficient and extremely specific. Commonly used DNA detection techniques (radiochemical, enzymatic and fluorescent) are based on the detection of various labels or reagents and have been proven to be time consuming, expensive and complex to implement. For fast, simple and inexpensive detection, direct methods are required. In the following, we want to introduce the recently achieved results with respect to field effect and voltammetric sensing, using single-crystalline CVD diamond as transducer.

3.6.1. DNA-FET. Diamond ISFET show sensitive variation of pH with approximately 55 mV/pH (Nebel *et al.* 2006*c*). This is close to the Nernst limit of 60 mV/pH. The effect arises from transfer doping so that no gate-insulator layer is required. The separation of surface channel and electrolyte is therefore very small. The application of such a FET system for DNA hybridization detection is new and we show in the

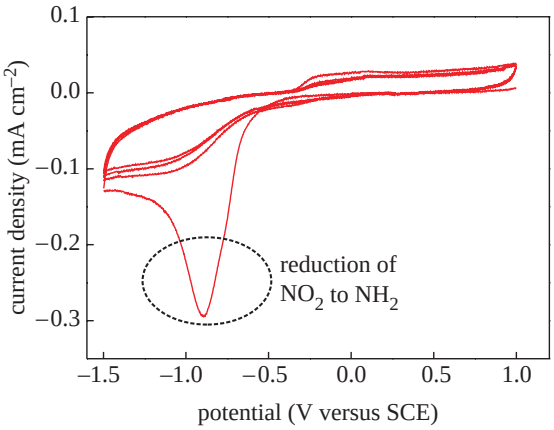

Figure 31. Cyclic voltammograms of 4-nitrophenyl-modified, highly B-doped single-crystalline diamond film in 0.1 M KCl solution with 10 : 90 (v/v) EtOH–H_2O. Scan rate: 0.1 V s^{-1}.

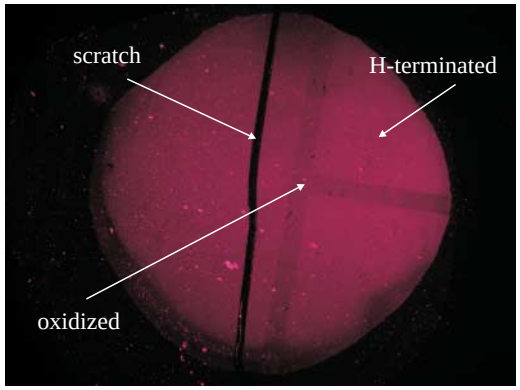

Figure 32. Fluorescence microscopy (FM) image of a DNA-functionalized single-crystalline diamond electrode after DNA hybridization with complementary oligonucleotides. The layer was originally H-terminated, but a T-shape has been oxidized.

following some typical results, achieved on structures with 10^{12}–10^{13} cm^{-2} ss-DNA markers bonded to diamond. A schematic figure of the device with hybridized ds-DNA is shown in figure 35. We used 1 M NaCl solution (containing 0.1 M phosphate with pH 7.2) with a Debye length of 3 Å as calculated by Poghossian *et al.* (2005),

$$\lambda_D = \left(\frac{\varepsilon_{el}\varepsilon_o kT}{2z^2q^2I}\right)^{1/2},$$

where k is the Boltzmann constant, T is the absolute temperature, ε_o is the permittivity of vacuum, ε_{el} is the dielectric constant of the electrolyte, z is the valency of ions in the electrolyte, q is the elementary charge and I represents the ionic strength; for a 1–1 salt, it can be replaced by the electrolyte concentration n_o. As the linker molecule is 12 Å (amine) and the cross-linker is 5 Å long, the DNA is not in touch with the Helmholtz layer in our experiments.

Figure 36*a* shows a comparison of drain–source currents (I_{DS}) measured at a fixed drain–source potential of −0.5 V as a function of gate potential (i) for ss-DNA marker molecules attached on the gate, (ii) for hybridized marker and target DNA on the gate, and (iii) after the removal of DNA from the diamond.

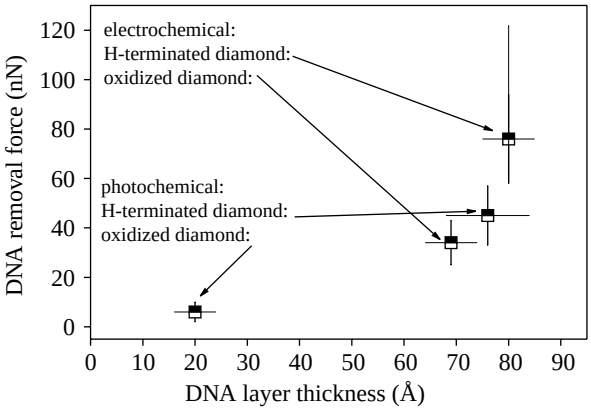

Figure 33. Comparison of critical removal forces of electrochemically attached DNA on H-terminated and oxidized diamond and of photochemically attached DNA on H-terminated and oxidized diamond.

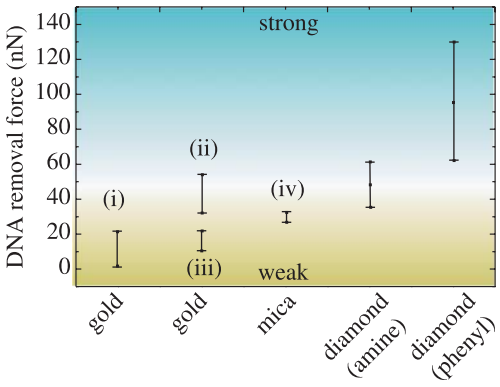

Figure 34. Comparison of DNA removal forces as detected in our experiments on diamond and compared with DNA bonding to Au (i: Xu *et al.* 1999; ii: Zhou *et al.* 2002; iii: Schwartz 2001) and mica (iv: Crampton *et al.* 2005).

The initial ss-DNA density bonded to diamond is $4\times10^{12}\,\mathrm{cm}^{-2}$. The drain–source current increases by hybridization as detected also for a sensor, where the initial ss-DNA density is slightly smaller ($10^{12}\,\mathrm{cm}^{-2}$) or larger ($10^{13}\,\mathrm{cm}^{-2}$). The gate potential variations from ss-DNA to complementary ds-DNA bonding vary between 30 and100 mV as shown in figure 36*b*. There is a clear trend that with decreasing DNA density, the potential shift becomes larger (as predicted by Poghossian *et al.* 2005). Taking into account the ion sensitivity of diamond ISFETs of 55 mV/pH, this reflects a decrease of pH of the buffer solution of approximately 1–1.4 by hybridization. Poghossian *et al.* (2005) have calculated that the average ion concentration within the intermolecular spaces after hybridization can be more than 3–4 times higher for cations than before hybridization. In the case of a Nernstian slope of the sensor, they predict a gate potential shift of 28–35 mV. Our results indicate a stronger change. The increase in drain–source current with hybridization can be well described by the transfer doping model as the increase in cation density will cause a decrease in pH. Therefore, the chemical potential will increase giving rise to the enhanced surface conductivity.

A summary of the published sensitivities of DNA-FETs from silicon is shown in figure 37 (data from Poghossian *et al.* 2005; Ishige *et al.* 2006; Yang *et al.* 2006). The initially reported sensitivities before 2004 of more than 100 meV threshold potential shifts by hybridization are not reproduced. Moreover, sensitivities are decreasing towards experimentally reproducible as well as theoretically predictable values in the range of 30–80 meV.

3.6.2. Cyclic voltammetry. For amperometric detection of DNA hybridization, we use $\mathrm{Fe(CN_6)}^{3-/4-}$ as mediator redox molecule (Kelley *et al.* 1999). The detection principle is shown in figure 38. In the case of ss-DNA bonded to diamond, the relatively small negatively charged redox molecules can diffuse through the layer of DNA and interact with the diamond electrode to cause a redox current. By hybridization of DNA, the intermolecular space shrinks, which leads to Coulomb repulsion between negatively charged $\mathrm{Fe(CN_6)}^{3-/4-}$ and negatively charged sugar–phosphate backbones of hybridized DNA. The redox reaction with diamond will therefore decrease (figure 38*b*).

The result is shown in figure 39, where we used cyclic voltammetry on H-terminated metallically doped (p-type) single-crystalline diamond in 0.5 mM $\mathrm{Fe(CN_6)}^{3-/4-}$, 100 mM KCl and 100 mM $\mathrm{KNO_3}$ measured with respect to Ag/AgCl with a scan rate of $100\,\mathrm{mV\,s}^{-1}$. The H-terminated diamond shows a well-pronounced oxidation peak at +280 mV and a corresponding reduction wave with a peak at +126 mV (not shown here). These characteristics are well known and have been published in the literature (Granger *et al.* 1999; Shin *et al.* 2005). After electrochemical attachment of phenyl linker molecules and ss-DNA marker molecules, the redox amplitude is decreasing to approximately 30% of the clean diamond surface. The peaks are not significantly shifted in potential or broadened by chemical modifications of the electrode (figure 39). By hybridization, peaks are slightly shifted towards higher oxidation and lower reduction potentials. The change in amplitude is approximately $50\,\mu\mathrm{A\,cm}^{-2}$. This change in voltammetric signal is reproducible and can be detected for several hybridization/denaturation cycles. This is the first report of voltammetric detection of DNA hybridization and denaturation on diamond using $\mathrm{Fe(CN_6)}^{3-/4-}$ as a mediator. It is clear that this technique needs to be characterized in depth to evaluate the sensitivity, durability and reproducibility of this sensor array.

Yang *et al.* (2004) reported about cyclic voltammetry experiments using $\mathrm{Fe(CN_6)}^{3-/4-}$ on boron-doped nanocrystalline diamond films coated with amines as linker and DNA. After ss-DNA marker attachment, their redox currents decreased drastically and they concluded that the application of cyclic voltammetry is inhibited by the highly insulating nature of the molecular amine layer linking DNA molecules to diamond. Our voltammetric experiments show that a detailed control of phenyl molecule deposition is required. Insulating properties with respect to $\mathrm{Fe(CN_6)}^{3-/4-}$ are detected if the phenyl

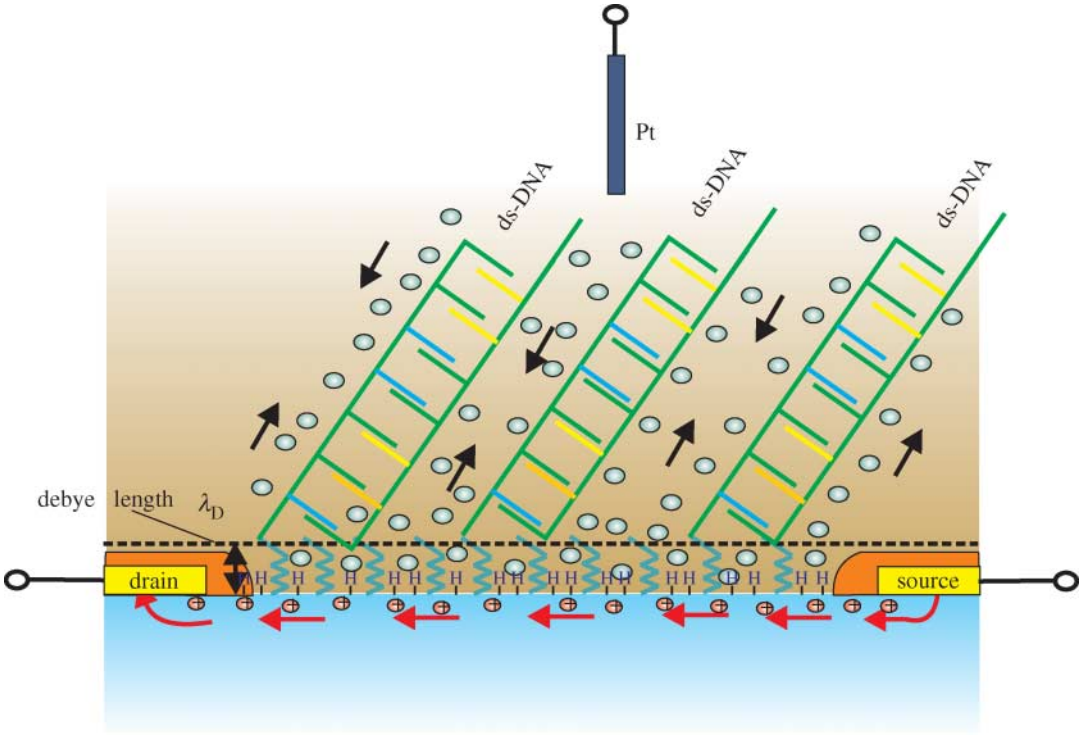

Figure 35. Schematic description of DNA hybridized on diamond DNA-FET sensor. The surface conductivity of diamond will be changed by the enhanced compensating cation density which arises by the negatively charged backbone structure of DNA. The 1 M NaCl buffer shirks the Debye length in our experiments to approximately 3 Å.

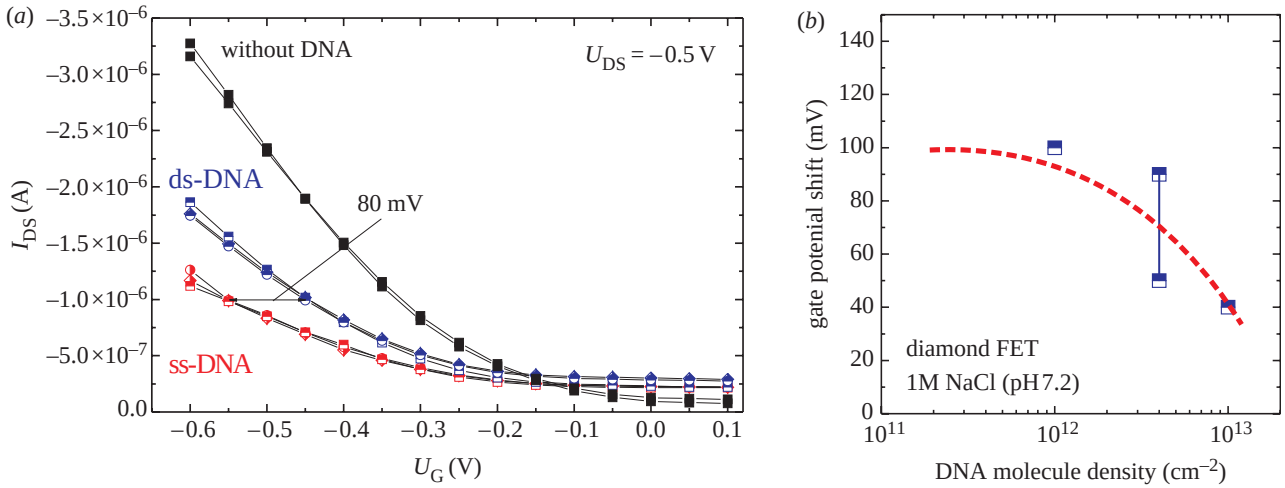

Figure 36. (*a*) Drain–source current variations measured as a function of gate potential at a fixed drain–source potential of −0.5 V for ss-DNA (marker DNA), after hybridization with complementary target ss-DNA to form ds-DNA and after removal of DNA by washing. A gate potential shift of approximately 80 mV is detected on this DNA-FET with approximately 4×10^{12} cm^{-2} molecules bonded to the gate. (*b*) Gate potential shifts as detected on diamond transistor structures with 10^{12}, 4×10^{12} and 10^{13} cm^{-2} ss-DNA marker molecules bonded to the gate area. The threshold potential is increasing towards less dense grafted diamond gates areas.

layer grows slowly and thick to form a dense scaffold on diamond. By short-time attachment, using constant potential attachment technique, dispersed layers are generated so that diffusion of $Fe(CN_6)^{3-/4-}$ is not suppressed.

Alternatively, Yang *et al.* (2004) and Hamers *et al.* (2005) applied impedance spectroscopy, where they detected hybridization-induced variations at high frequency as shown in figure 40. A clear difference between single-stranded DNA bonded to diamond and double-stranded DNA is detected.

4. BONDING AND DETECTION OF ENZYMES AND PROTEINS ON DIAMOND

After establishment of surface functionalization techniques for diamond using photo- and electrochemical means, bonding of molecules like enzymes (Song *et al.* 2004) and proteins (Härtl *et al.* 2004) has been demonstrated relatively faster. As the use of carbon-based transducers for biosensing glassy carbon, highly oriented pyrolytic graphite and diamonds like carbon- and boron-doped diamonds is well established in

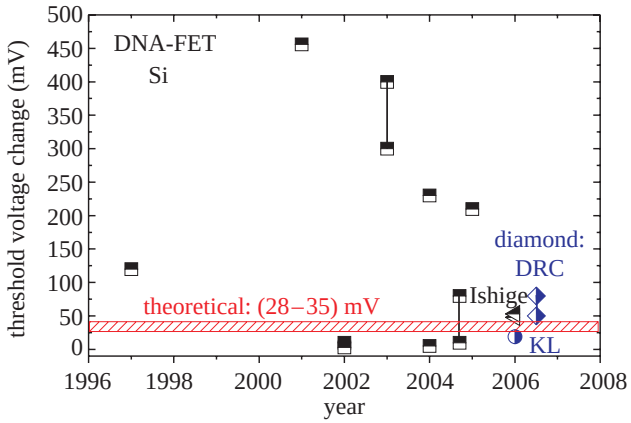

Figure 37. Comparison of silicon-based DNA field-effect transistor sensitivities as a function of time (half filled squares from Poghossian *et al.* 2005 and half-filled triangles from Ishige *et al.* 2006) with diamond sensitivities as shown (half-filled diamonds, DRC) and with diamond-related data from Yang *et al.* (2006) (half-filled circle). The shaded area indicates the theoretically predicted sensitivity, following the model of Poghossian *et al.* (2005).

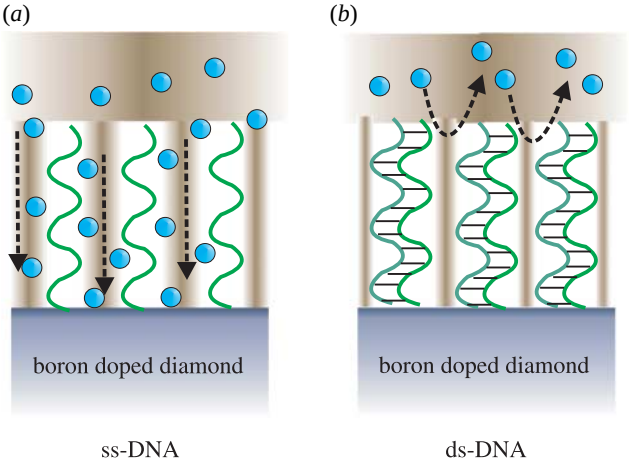

Figure 38. Schematic DNA hybridization detection mechanism using $Fe(CN_6)^{3-/4-}$ as mediator redox molecules. In the case of ss-DNA, the negatively charged redox molecules $Fe(CN_6)^{3-/4-}$ (blue balls) can diffuse through the DNA layer. After hybridization, the space between individual ds-DNA molecules becomes too small for negatively charged molecules to overcome the repulsive Coulomb forces from the negatively charged backbone of ds-DNA.

electrochemistry, increasing biosensing applications of such materials can be expected. While the past has been dominated to find chemical treatments to achieve surface modifications of diamond, the future will be dominated by optimization of multilayer structures for biosensing.

5. SUMMARY

In this review, we have summarized the recently achieved results with respect to photo- and electrochemical surface modifications of diamond. Both techniques have been optimized to a level, which allowed the realization of first generation electrochemical and

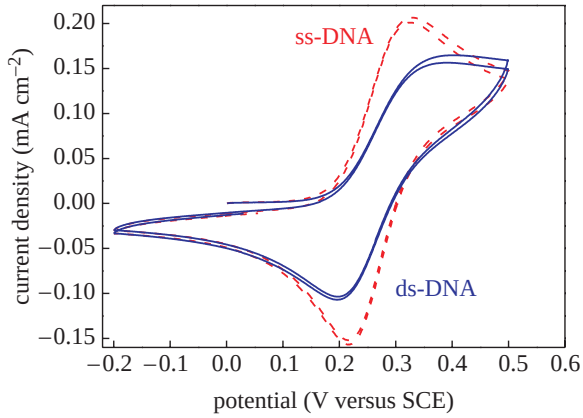

Figure 39. Cyclic voltammograms on ss- and ds-DNA grafted, metallically boron-doped (p-type) single-crystalline diamond in 0.5 mM $Fe(CN_6)^{3-/4-}$, 100 mM KCl and 100 mM KNO_3 measured with respect to Ag/AgCl with a scan rate of 100 mV s^{-1}. The oxidation and reduction peaks are decreasing to approximately 50 µA cm^{-2} by hybridization.

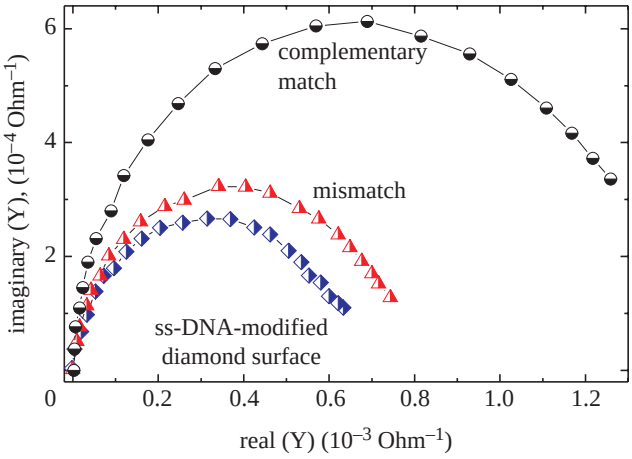

Figure 40. Impedance spectroscopic properties of DNA-modified nanodiamond films. The admittance (inverse impedance) is shown in the complex plane as detected for ss-DNA, for exposure to mismatched DNA and after exposure to complementary DNA (for details see Hamers *et al.* 2005).

field-effect DNA sensors. By AFM experiments, we detect a formidable bonding stability of biomolecular arrangements on diamond. It confirms earlier reports by Yang *et al.* (2002) about exceptional DNA-bonding stability in hybridization cycles. Applications of diamond biosensors in high-throughput systems, where especially high bonding stability is required, will therefore be of significant interest in the future. Our experiments also show that basic understanding of growth mechanisms and electronic and chemical properties of each layer of the composite biorecognition film (e.g. amine/cross-linker/ss-DNA) is required to achieve progress with respect to optimization of sensor performance.

Finally, the proper selection of 'diamond transducer materials' for biosensor applications is of comparable importance. Electronic detection of bonding events in electrolyte solutions requires high-quality diamond with minimized defect densities, no grain boundaries and no sp^2, and with a defect-free surface termination.

Such diamond transducers are and will be more expensive than established semiconducting materials like Si. Therefore, we assume that future applications of diamond will be in clinical, high-throughput systems which require high bonding stability. Multiarray sensors from single-crystalline diamond can be realized using established technologies and chemistry. As prices for established DNA multiarray optical sensors are rather expensive (typically more than 5000€; see http://www.affymetrix.com), the costs for diamond substrates of typically 150–250€ will not be a strong argument against the use of diamond for such applications. In any case, diamond needs to show that its device properties and performances are superior compared with other transducer layers to be commercially successful.

There are several fields where nano- and polycrystalline diamond seems to become a promising leading application. Nano-size diamond particles with a diameter of typically 100 nm are currently investigated as core material for rapid, low volume solid-phase extraction of analytes, including proteins and DNA from a variety of biological samples. These particles are unique as they are optically transparent, carry specific functional groups and can mix rapidly with sample solutions upon agitation. After extraction of the target analyte by the particles, the particles can be recollected and analysed. Second, nanodiamond can be used as 'colour-centre' marker as it has several interesting defect-related light emitting centres (colour centres) like the nitrogen–vacancy (N–V) complex and others, which makes nanodiamond unique with respect to the FM applications. These colour-centres are resistant against photobleaching and can be consumed by mammalian cells with minimal cytotoxicity (Chang *et al.* 2006).

The increasing demand for secure, mobile, wireless communication has stimulated interest in technologies capable of reducing the size and power consumption of wireless modules and enhancing the bandwidth efficiency of communication networks. Nanodiamond micro-electrical-mechanical-systems (MEMSs) are at the leading etch of this field as the frequency (f) and quality (Q) product of such nanodiamond oscillators reached $f=1.51$ GHz and the quality factor $Q=11\,555$ (Sekaric *et al.* 2002; Wang *et al.* 2002, 2004). In the field of biosensing, such high-quality mechanical oscillation systems are also of significant importance for improved detection and sensibility (see for example Braun *et al.* 2005; Ilic *et al.* 2005).

Direct manipulation of living cells or transfer of molecules into cells ('cell surgery') is an emerging and increasingly important technology in biology. It requires new tools with dimensions below the micrometre regime. A typical gene surgery tip should be approximately 40 µm long with a diameter of around 400 nm (for a review see Han *et al.* 2005). In addition, the material should not poison the cell during manipulation, the surface should be optimized with respect to friction of cell membranes and it should allow the application of given potentials to the tip to electrostatically bond or release DNA fragments. These are the sophisticated requirements currently under investigations. One of the best candidates is nanocrystalline diamond, as it has the required mechanical stability (hardness 50 100 GPa), the surface can be adjusted to optimize friction and, if properly designed, the core of the tip can be conductive by boron doping.

Based on these arguments, we are convinced that bioapplication of diamond, either monocrystalline for electronic sensing or poly- and nanocrystalline for mechanical techniques, are very realistic opportunities for this promising material. Diamond will surely find its place in the rapidly growing field of biology and biotechnology. Whether diamond will be the material of choice for biosensors will depend on the outcome of these research activities. The window of opportunity for diamond is now wide open; however, to compete with other transducer materials, which are cheaper, less sophisticated in growth and compatible with silicon technology, will require optimized use of core advantages of diamond: (i) chemical stability, (ii) strong bonding of organic molecules, (iii) low electrochemical background current, (iv) wide electrochemical potential window, (v) no gate-insulator for DNA-FETs from diamond, and (vi) perfect surface electronic properties which includes control of interfacial energy alignments by H- or O-termination to optimize electron-transfer reactions.

The authors want to thank T. Nakamura for the synthesis of TFAAD molecules, which contributed significantly to our progress, as well as to T. Yamamoto, who helped to fabricate DNA-FET detectors. The authors also want to thank Dr Park, who supported their activities with an electrochemical analyser system, and Wiley-VCH Verlag GmbH&Co KG for copyright transfer of figures 6, 7, 16–22, 24, 32 and 33 that are published in a recently printed review of *Phys. Stat. Sol.* (a) **203** (13), 3245–3270 (2006).

REFERENCES

Allongue, P., Henry de Villeneuve, C., Cherouvrier, G., Cortes, R. & Bernard, M.-C. 2003 Phenyl layers on H–Si(111) by electrochemical reduction of diazonium salts: monolayer versus multilayer formation. *J. Electroanal. Chem.* **550–551**, 161–174. (doi:10.1016/S0022-0728(03)00076-7)

Angus, J. C., Pleskov, Y. V. & Eaton, S. C. 2004 Electrochemistry of diamond. In *Thin film diamond II*, vol. 77 (eds C. E. Nebel & J. Ristein) *Semiconductors and semimetals*, p. 97. Amsterdam, The Netherlands; New York, NY: Elsevier; Academic Press.

Bergonzo, P. & Jackman, R. 2004 Diamond-based radiation and photon detectors. In *Thin-film diamond I*, vol. 76 (eds C. E. Nebel & J. Ristein) *Semiconductors and semimetals*, pp. 197–309. Amsterdam, The Netherlands: Elsevier.

Bergonzo, P., Tromson, D. & Mer, C. 2003 Radiation detection devices made from CVD diamond. *Semicond. Sci. Technol.* **18**, S105–S112. (doi:10.1088/0268-1242/18/3/315)

Borst, T. H. & Weis, O. 1996 Boron-doped homoepitaxial diamond layers: fabrication, characterization, and electronic applicationssol. *Phys. Status Solidi A* **154**, 423–444.

Bousse, L., de Rooji, N. F. & Bergeveld, P. 1983 Operation of chemically sensitive field-effect sensors as a function of the insulator electrolyte interface. *IEEE Trans. Electron Dev.* **30**, 1263–1270.

Braun, T., Barwich, V., Ghatkesar, M. K., Bredekamp, A. H., Gerber, C., Hegner, M. & Lang, H. P. 2005 Micromechanical mass sensors for biomolecular detection in physiological environment. *Phys. Rev. E* **72**, 31 907. (doi:10.1103/PhysRevE.72.031907)

Brawer, M. K. 2001 *Prostate specific antigen*. New York, NY: Marcel Dekker.

Buriak, J. M. 2002*a* Organometallic chemistry on silicon and germanium surfaces. *Chem. Rev.* **102**, 1271–1308. (doi:10.1021/cr000064s)

Buriak, J. M. 2002*b* Organometallic chemistry on silicon and germanium surfaces. *Chem. Rev.* **102**, 1271–1308. (doi:10.1021/cr000064s)

Carlisle, J. A. & Auciello, O. 2003 Ultrananocrystalline diamond. *Electrochem. Soc. Interface* **12**, 28–31.

Chang, H.-C., Chen, K. W. & Kwok, S. 2006 Nanodiamond as a possible carrier of extended red emission. *Astrophys. J.* **639**, L63–L66. (doi:10.1086/502677)

Cicero, R. L., Chidsey, E. D., Lopinski, G. P., Wayner, D. D. M. & Wolkow, R. A. 2002 Olefin additions on H–Si(111): evidence for a surface chain reaction initiated at isolated dangling bonds. *Langmuir* **18**, 305–307. (doi:10.1021/la010823h)

Collins, A. T., Dean, P. J., Lightowler, E. C. & Sherman, W. F. 1965 Acceptor-impurity infrared absorption in semiconducting synthetic diamond. *Phys. Rev.* **140**, A1272–A1274. (doi:10.1103/PhysRev.140.A1272)

Cui, J. B., Ristein, J. & Ley, L. 1998 Electron affinity of the bare and hydrogen covered single crystal diamond (111) surface. *Phys. Rev. Lett.* **81**, 429–432. (doi:10.1103/PhysRevLett.81.429)

Crampton, N., Bonass, W. A., Kirkham, J. & Thomson, N. H. 2005 Formation of aminosilane-functionalized mica for atomic force microscopy imaging of DNA. *Langmuir* **21**, 7884–7891. (doi:10.1021/la050972q)

Erts, D., Polyakov, B., Olin, H. & Tuite, E. 2003 Spatial and mechanical properties of dilute DNA monolayers on gold imaged by AFM. *J. Phys. Chem. B* **107**, 3591–3597. (doi:10.1021/jp0261657)

Etzioni, R., Urban, N., Ramsey, S., McIntosh, M., Schwartz, S., Reid, B., Radich, J., Anderson, G. & Hartwell, L. 2003 The case of early detection. *Nat. Rev. Cancer* **3**, 243–252. (doi:10.1038/nrc1041)

Fujishima, A., Einaga, Y., Rao, T. N. & Tryk, D. A. 2005 *Diamond electrochemistry*. Amsterdam, The Netherlands; Tokyo, Japan: Elsevier; BKC.

Gi, R. S., Mizumasa, T., Akiba, Y., Hirose, Y., Kurosu, T. & Iida, M. 1995 Formation mechanism of p-type surface conductive layer on deposited diamond films. *Jpn J. Appl. Phys.* **34**, 5550–5555. (doi:10.1143/JJAP.34.5550)

Granger, M. C., Xu, J., Strojek, J. W. & Swain, G. M. 1999 Polycrystalline diamond electrodes: basic properties and applications as amperometric detectors in flow injection analysis and liquid chromatography. *Anal. Chim. Acta* **397**, 145–161. (doi:10.1016/S0003-2670(99)00400-6)

Granger, M. C. *et al.* 2000 Standard electrochemical behavior of high-quality, boron-doped polycrystalline diamond thin-film electrodes. *Anal. Chem.* **72**, 3793–3804. (doi:10.1021/ac0000675)

Hamers, J. R., Butler, J. E., Lasseter, T., Nichols, B. M., Russell Jr, J. N., Tse, K.-Y. & Yang, W. 2005 Molecular and biomolecular monolayers on diamond as an interface to biology. *Diamond Relat. Mater.* **14**, 661–668. (doi:10.1016/j.diamond.2004.09.018)

Han, S. W., Nakamura, C., Obataya, I., Nakamura, N. & Miyake, J. 2005 Gene expression using an ultrathin needle enabling accurate displacement and low invasiveness. *Biochem. Biophys. Res. Commun.* **332**, 633–639. (doi:10.1016/j.bbrc.2005.04.059)

Härtl, A. *et al.* 2004 Protein-modified nanocrystalline diamond thin films for biosensor applications. *Nat. Mater.* **3**, 736–742. (doi:10.1038/nmat1204)

Hashimoto, K., Ito, K. & Ishimori, Y. 1994 Sequence-specific gene detection with a gold electrode modified with DNA probes and an electrochemical active dye. *Anal. Chem.* **66**, 3830–3833. (doi:10.1021/ac00093a045)

Ilic, B., Yang, Y., Aubin, K., Reichenbach, R., Krylov, S. & Craighead, H. G. 2005 Enumeration of DAN molecules bound to nanomechanical oscillator. *Nano Lett.* **5**, 925–929. (doi:10.1021/nl050456k)

Ishige, Y., Shimoda, M. & Kamahori, M. 2006 Immobilization of DNA probes onto gold surface and its application to fully electric detection of DNA hybridization using field effect transistor sensor. *Jpn J. Appl. Phys.* **45**, 3776–3783. (doi:10.1143/JJAP.45.3776)

Jackman, R. (ed.) 2003 Diamond electronics. *Semicond. Sci. Technol.* **18**, S86–S95

Kelley, S. O., Boon, E. M., Barton, J. K., Jackson, N. M. & Hill, M. G. 1999 Single-base mismatch detection based on charge transduction through DNA. *Nucleic Acids Res.* **27**, 4830–4837. (doi:10.1093/nar/27.24.4830)

Koizumi, S., Kamo, M., Sato, Y., Ozaki, H. & Inuzuka, T. 1997 Growth and characterization of phosphorous doped {111} homoepitaxial diamond thin films. *Appl. Phys. Lett.* **71**, 1065–1067. (doi:10.1063/1.119729)

Kondo, T., Einaga, Y., Sarada, B. V., Rao, T. N., Tryk, D. A. & Fujishima, A. 2002 Homoepitaxial single-crystal boron-doped diamond electrodes for electroanalysis. *J. Electrochem. Soc.* **149**, E179–E184. (doi:10.1149/1.1471548)

Kono, S., Shiraishi, M., Goto, T., Abukawa, T., Tachiki, M. & Kawarada, H. 2005 An electron-spectroscopic view of CVD diamond surface conductivity. *Diamond Relat. Mater.* **14**, 459–465. (doi:10.1016/j.diamond.2004.11.011)

Kremsky, J. N., Wooters, J. L., Dougherty, J. P., Meyers, R. E., Collins, M. & Brown, E. L. 1987 Immobilization of DNA via oligonucleotides containing an aldehyde or carboxylic-acid group at the 5′ terminus. *Nucleic Acids Res.* **15**, 2891–2909.

Landstrass, M. I. & Ravi, K. V. 1998 Resistivity of chemical vapor-deposited diamond films. *Appl. Phys. Lett.* **55**, 975–977. (doi:10.1063/1.101694)

Linford, M. R., Fenter, P., Eisenberg, P. M. & Chidsay, C. E. D. 1995 Alkyl monolayers on silicon prepared from 1-alkenes and hydrogen-terminated silicon. *J. Am. Chem. Soc.* **117**, 3145–3155. (doi:10.1021/ja00116a019)

Maier, F., Riedel, M., Mantel, B., Ristein, J. & Ley, L. 2000 Origin of surface conductivity in diamond. *Phys. Rev. Lett.* **85**, 3472–3475. (doi:10.1103/PhysRevLett.85.3472)

Millan, K. M., Spurmanis, A. J. & Mikkelsen, S. R. 1992 Covalent immobilization of DNA into glassy-carbon electrodes. *Electroanalysis* **4**, 929–932. (doi:10.1002/elan.1140041003)

Nazare, M. H. & Neves, A. J. 2001 Properties, growth and applications of diamond, (eds) EMIS Datareview Series No. 26, INSPEC publication.

Nebel, C. E. 2003*a* Electronic properties of CVD diamond. *Semicond. Sci. Technol.* **18**, S1–S11. (doi:10.1088/0268-1242/18/3/301)

Nebel, C. E. 2003*b* Transport and defect properties of intrinsic and boron-doped diamond. In *Thin-film diamond I* (eds C. E. Nebel & J. Ristein) *Semiconductors and semimetals*, 76, p. 261. Amsterdam, The Netherlands: Elsevier.

Nebel, C. E. 2005 Surface transfer-doping of H-terminated diamond with adsorbates. *New Diamond Front. Carbon Technol.* **15**, 247–264.

Nebel, C. E. & Ristein, J. (eds) 2003 *Thin-film diamond I Semiconductors and semimetals*, vol. 76. Amsterdam, The Netherlands; New York, NY: Elsevier; Academic Press.

Nebel, C. E. & Ristein, J. (eds) 2004 *Thin-film diamond II Semiconductors and semimetals*, vol. 77. Amsterdam, The Netherlands; New York, NY: Elsevier; Academic Press.

Nebel, C. E., Kato, H., Rezek, B., Shin, D., Takeuchi, D., Watanabe, H. & Yamamoto, T. 2006*a* Electrochemical properties of undoped hydrogen terminated CVD diamond. *Diamond Relat. Mater.* **15**, 264–268. (doi:10.1016/j.diamond.2005.08.012)

Nebel, C. E., Rezek, B., Shin, D., Watanabe, H. & Yamamoto, T. 2006*b* Electronic properties of H-terminated diamond in electrolyte solutions. *J. Appl. Phys.* **99**, 33 711. (doi:10.1063/1.2171805)

Nebel, C. E., Rezek, B., Shin, D. & Watanabe, H. 2006*c* Surface electronic properties of H-terminated diamond in contact with adsorbates and electrolytes. *Phys. Status Solidi A* **203**, 3273–3298. (doi:10.1002/pssa.200671401)

Nebel, C. E., Shin, D., Takeuchi, D., Yamamoto, T., Watanabe, H. & Nakamura, T. 2006*d* Photochemical attachment of amine linker molecules on hydrogen terminated diamond. *Diamond Relat. Mater.* **15**, 1107–1112. (doi:10.1016/j.diamond.2005.11.041)

Nebel, C. E., Shin, D., Takeuchi, D., Yamamoto, T., Watanabe, H. & Nakamura, T. 2006*e* Alkene/diamond liquid/solid interface characterization using internal photoemission spectroscopy. *Langmuir* **22**, 5645–5653. (doi:10.1021/la052685s)

Nesladek, M., Haenen, K. & Vanecek, M. 2003 In *Thin-film diamond I,* vol. 76 (eds C. E. Nebel & J. Ristein) *Semiconductors and semimetals*, p. 325. Amsterdam, The Netherlands: Elsevier.

Nichols, B. M., Butler, J. E., Russel Jr, J. N. & Hamers, R. J. 2005 Photochemical functionalization of hydrogen-terminated diamond surfaces: a structural and mechanistic study. *J. Phys. Chem. B* **109**, 20 938–20 947. (doi:10.1021/jp0545389)

Okushi, H. 2001 High quality homoepitaxial CVD diamond for electronic devices. *Diamond Relat. Mater.* **10**, 281–288. (doi:10.1016/S0925-9635(00)00399-X)

Pinson, J. & Podvorica, F. 2005 Attachment of organic layers to conductive or semiconductive surfaces by reduction of diazonium salts. *Chem. Soc. Rev.* **34**, 429–439. (doi:10.1039/b406228k)

Pleskov, Y. V., Evstefeeva, Y. E., Krotova, M. D., Elkin, V. V., Mazin, V. M., Mishuk, V. Y., Varnin, V. P. & Teremetskaya, I. G. 1998 Synthetic semiconductor diamond electrodes: the comparative study of the electrochemical behaviour of polycrystalline and single crystal boron-doped films. *J. Electroanal. Chem.* **455**, 139–146. (doi:10.1016/S0022-0728(98)00175-2)

Poghossian, A., Cherstvy, A., Ingebrandt, S., Offenhaeusser, A. & Schoening, M. J. 2005 Possibilities and limitations of label-free detection of DNA hybridization with field-effect-based devices. *Sens. Actuators, B* **111–112**, 470–480. (doi:10.1016/j.snb.2005.03.083)

Rasmussen, S. R., Larsen, M. R. & Rasmussen, S. E. 1991 Covalent immobilization of DNA onto polystyrene microwells—the molecules are only bound at the 5′ end. *Anal. Biochem.* **198**, 138–142. (doi:10.1016/0003-2697(91)90518-X)

Rezek, B., Shin, D., Nakamura, T. & Nebel, C. E. 2006 Geometric properties of covalently bonded DNA on single-crystal line diamond. *J. Am. Chem. Soc.* **128**, 3884–3885. (doi:10.1021/ja058181y)

Sander, C. 2000 Genomic medicine and the future of health care. *Science* **287**, 1977–1978. (doi:10.1126/science.287.5460.1977)

Schwartz, P. V. 2001 Meniscus force nanografting: nanoscopic patterning of DNA. *Langmuir* **17**, 5971–5977. (doi:10.1021/la001625d)

Sekaric, L., Parpia, J. M., Craighead, H. G., Feygelson, T., Houston, B. H. & Butler, J. E. 2002 Nanomechanical resonant structures in nanocrystalline diamond. *Appl. Phys. Lett.* **81**, 4455–4457. (doi:10.1063/1.1526941)

Shin, D., Watanabe, H. & Nebel, C. E. 2005 Insulator–metal transition of intrinsic diamond. *J. Am. Chem. Soc.* **127**, 11 236–11 237. (doi:10.1021/ja052834t)

Shin, D. C., Tokuda, N., Rezek, B. & Nebel, C. E. 2006 Periodically arranged benzene-linker molecules on boron-doped single-crystalline diamond films for DNA sensing. *Electrochem. Commun.* **8**, 844–850. (doi:10.1016/j.elecom.2006.03.014)

Shirafuji, J. & Sugino, T. 1996 Electrical properties of diamond surfaces. *Diamond Relat. Mater.* **5**, 706–713. (doi:10.1016/0925-9635(95)00415-7)

Song, K. S., Degawa, M., Nakamura, Y., Kanazawa, H., Umezawa, H. & Kawarada, H. 2004 Surface-modified diamond field-effect transistors for enzyme-immobilized biosensors. *Jpn J. Appl. Phys., Part 2* **43**, L814–L817. (doi:10.1143/JJAP.43.L814)

Sque, S. J., Jones, R. & Briddon, P. R. 2006 Structure, electronics, and interaction of hydrogen and oxygen on diamond surfaces. *Phys. Rev. B* **73**, 085313. (doi:10.1103/PhysRevB.73.085313)

Srinivas, P. R., Kramer, B. S. & Srivastava, S. 2001 Trends in biomarker research for cancer detection. *Lancet Oncol.* **2**, 698–704. (doi:10.1016/S1470-2045(01)00560-5)

Strother, T., Cai, W., Zhao, X. S., Hamers, R. J. & Smith, L. M. 2000 Synthesis and characterization of DNA-modified silicon (111) surfaces. *J. Am. Chem. Soc.* **122**, 1205–1209. (doi:10.1021/ja9936161)

Swain, G. M. 2004 Electroanalytical applications of diamond electrodes. In *Thin film diamond II,* vol. 77 (eds C. E. Nebel & J. Ristein) *Semiconductors and semimetals*, p. 121. Amsterdam, The Netherlands; New York, NY: Elsevier; Academic Press.

Takahashi, K., Tanga, M., Takai, O. & Okamura, H. 2000 DNA bonding to diamond. *Bio Ind.* **17**, 44–51.

Takahashi, K., Tanga, M., Takai, O. & Okamura, H. 2003 DNA preservation using diamond chips. *Diamond Relat. Mater.* **12**, 572–576. (doi:10.1016/S0925-9635(03)00070-0)

Takeuchi, D., Yamanaka, S., Watanabe, H., Sawada, S., Ichinose, H., Okushi, H. & Kajimura, K. 1999 High quality homoepitaxial diamond thin film synthesis with high growth rate by a two-step growth method. *Diamond Relat. Mater.* **8**, 1046–1049. (doi:10.1016/S0925-9635(99)00002-3)

Takeuchi, D., Kato, H., Ri, G. S., Yamada, T., Vinod, P. R., Hwang, D., Nebel, C. E., Okushi, H. & Yamasaki, S. 2005 Direct observation of negative electron affinity in hydrogen-terminated diamond surfaces. *APL* **86**, 152 103.

Tang, L., Tsai, C., Gerberich, W. W., Kruckeberg, L. & Kania, D. R. 1995 Biocompatibility of chemical-vapor-deposited diamond. *Biomaterials* **16**, 483–488. (doi:10.1016/0142-9612(95)98822-V)

Wang, J., Butler, J. E., Hsu, D. S. Y. & Nguyen, C. C.-T. 2002 High-Q micromechanical resonators in CH_4-reactant-optimized high acoustic velocity CVD polydiamond. In *Solid State Sensor, Actuator, and Microsystems Workshop Proceedings, Hilton Head Island, SC*, pp. 61–62.

Wang, J., Butler, J. E., Feygelson, T. & Nguyen, C. T.-C. 2004 1.51-GHz polydiamond micromechanical disk resonantor with impedance mismatch isolating support. In *Proc. 17th IEEE Micro Electro Mechanical Systems Conf., Maastrich*, pp. 641–644. The Netherlands, Jan. 25–29

Wang, J., Firestone, M. A., Auciello, O. & Carlisle, J. A. 2004 Functionalization of ultrananocrystalline diamond films by electrochemical reduction of aryldiazonium salts. *Langmuir* **20**, 11 450–11 456. (doi:10.1021/la048740z)

Watanabe, H., Takeuchi, D., Yamanaka, S., Okushi, H., Kajimura, K. & Sekiguchi, T. 1999 Homoepitaxial diamond film with an atomically flat surface over a large area. *Diamond Relat. Mater.* **8**, 1272–1276. (doi:10.1016/S0925-9635(99)00126-0)

Williams, O. A., Daenen, M., D'Haen, J., Haenen, K., Maes, J., Moshchalkov, V. V., Nesladek, M. & Gruen, D. M. 2006 Comparison of the growth and properties of ultrananocrystalline diamond and nanocrystalline diamond. *Diamond Relat. Mater.* **15**, 654–658. (doi:10.1016/j.diamond.2005.12.009)

Wulfkuhle, J. D., Liotta, L. A. & Petricoin, E. F. 2003 Proteomic applications for the early detection of cancer. *Nat. Rev. Cancer* **3**, 267–275. (doi:10.1038/nrc1043)

Xu, S., Miller, S., Laibinis, P. E. & Liu, G. Y. 1999 Fabrication of nanometer scale patterns within self-assembled monolayers by nanografting. *Langmuir* **15**, 7244–7251. (doi:10.1021/la9906727)

Yang, W. *et al.* 2002 DNA-modified nanocrystalline diamond thin-films as stable, biologically active substrates. *Nat. Mater.* **1**, 253–257. (doi:10.1038/nmat779)

Yang, W., Butler, J. E., Russel Jr, J. N. & Hamers, R. J. 2004 Interfacial electrical properties of DNA-modified diamond thin films: intrinsic response and hybridization-induced field effects. *Langmuir* **20**, 6778–6787. (doi:10.1021/la036460y)

Yang, J.-H., Song, K.-S., Kuga, S. & Kawarada, H. 2006 Characterization of direct immobilized probe DNA on partially functionalized diamond solution-gate field-effect transistors. *Jpn J. Appl. Phys.* **45**, L1114–L1117. (doi:10.1143/JJAP.45.L1114)

Zhang, G.-J., Song, K. S., Nakamura, Y., Ueno, T., Funatsu, T., Ohdomari, I. & Kawarada, H. 2006 DNA micropatterning on polycrystalline diamond via one-step direct amination. *Langmuir* **22**, 3728–3734. (doi:10.1021/la050883d)

Zhou, D. J., Sinniah, K., Abell, C. & Rayment, T. 2002 Use of atomic force microscopy for making addresses in DNA coatings. *Langmuir* **18**, 8278–8281. (doi:10.1021/la0258547)